N. A. F.

CERN 87-07
Vol. I
4 June 1987

ORGANISATION EUROPÉENNE POUR LA RECHERCHE NUCLÉAIRE
CERN EUROPEAN ORGANIZATION FOR NUCLEAR RESEARCH

PROCEEDINGS OF THE WORKSHOP ON PHYSICS AT FUTURE ACCELERATORS

La Thuile (Italy) and Geneva (Switzerland)
7 - 13 January 1987

Vol. I

GENEVA
1987

BEYOND THE STANDARD MODEL

SUMMARY REPORT OF THE PHYSICS-2 WORKING GROUP

V. Angelopoulos, P. Bagnaia, G. Barbiellini, R. Batley, D. Bloch, A. Blondel, W. Buchmüller, G. Burgers, R. Cashmore, P. Chiappetta, F. Cornet, C. Dionisi, M. Dittmar, J. Ellis, J.-Ph. Guillet, N. Harnew, P. Igo-Kemenes, R. Kleiss, H. Komatsu, H. Kowalski, B. Mansoulié, P. Méry, A. Nandi, F. Pauss, M. Perrottet, F. Renard, R. Rückl, A. Savoy-Navarro, D. Schaile, D. Schlatter, B. Schrempp, F. Schrempp, K. Schwarzer, N. Tracas, D. Treille, N. Wermes, D. Wyler, N. Zaganidis, P. Zerwas and F. Zwirner

Presented by J. Ellis and F. Pauss
CERN, Geneva, Switzerland

1. INTRODUCTION

This Working Group has tried to compare, on a similar basis, the possible contributions of all the different proposed accelerators (pp, ep, and e^+e^-) to the investigation of a selection of physics topics. Theorists have proposed a large number of ideas going beyond the Standard Model, not all of which could be explored within the constraints of time and people available. Table 1 shows the physics matrix of topics and accelerators which we have studied. Listed against each entry in the matrix are the persons who have worked on the corresponding accelerator. In this report we summarize their work, details of which can be found in individual contributions to appear in vol. II of these proceedings.

Among the subjects *not* discussed by our group are: technicolour; 'classical' additional neutral Z′ bosons as found in $SU(2)_L \times SU(2)_R \times U(1)$ models; right-handed currents; and additional charged W′ bosons. Our selection of topics has been guided in part by a quest for complementarity to previous studies [1, 2], and in part by a general theoretical perspective on Physics beyond the Standard Model which we now describe.

There is no confirmed experimental result that conflicts with the Standard Model, but this is well known to have many theoretical defects. Outstanding problems left unanswered by the Standard Model can be sorted into three main categories: Unification, Flavour, Mass. The Unification Problem consists in finding a simple mathematical framework that encompasses all the non-gravitational interactions [3]. A favoured approach is to look for a single non-Abelian group which includes the $SU(3)_c \times SU(2)_L \times U(1)_Y$ factors of the Standard Model. Such a Grand Unified Theory (GUT) makes predictions for $\sin^2\theta_w$, and perhaps for the bottom quark mass, exotic new phenomena such as proton decay, and magnetic monopoles. Unfortunately, the scale of Grand Unification must be at least 10^{15} GeV, which often makes the predictions for low-energy phenomena rather ambiguous, and renders GUTs difficult to test at accelerators. Consequently, our Working Group has not pursued this physics topic.

The Flavour Problem is that of understanding the number of matter species, and the ratios of their masses and of their weak charged-current couplings. A favoured approach is to suggest that quarks and leptons are composite, being made of more elementary constituents [4]. These preons would be bound on a distance of 10^{-16} cm or less, corresponding to an excitation energy of 1 TeV or more. Composite models of the massive vector bosons $W^\pm$ and Z^0 have also been proposed by analogy with the ϱ, ω, ϕ, etc. vector mesons of QCD, the motivation being to understand why these bosons are massive, unlike the photon γ and the gluon g. Among the signatures of such composite models would be new contact interactions with scale parameters $\Lambda \geq 1$ TeV, form factors, excited states, and new composite ground states, many of them exotic. The majority of such models predict new effects with $\Lambda \leq 10^2$ TeV, within the physics reach of the accelerators under discussion. Accordingly, composite models are extensively discussed in this report.

Table 1

Physics matrix and contributors[a)]

	pp	ep	e^+e^-
Supersymmetry	Batley Ellis Kowalski Mansoulié Pauss Savoy-Navarro Zaganidis	Komatsu Rückl	Dionisi Dittmar
Z′	Bagnaia Chiappetta Guillet Zwirner	Angelopoulos Cornet Rückl Tracas	Barbiellini Blondel Ellis Schlatter Tracas Treille Zerwas
Leptoquarks	Ellis Kowalski Rückl Zerwas	Buchmüller Cashmore Harnew Rückl Tracas Wyler	Igo-Kemenes Schaile Schrempp B. and F. Zerwas
Compositeness	Bagnaia Kleiss Nandi Wermes Zerwas	Cornet Rückl	Bloch Kleiss Méry Perrottet Renard Schrempp B. and F. Schwarzer Treille Wermes Zerwas

a) In addition, G. Burgers has compared the cross-sections for new particle production by e^+e^- annihilation and $\gamma\gamma$ collisions.

The problem of Mass is that of understanding the origins of the different elementary particle masses, and why the quark, lepton, W, and Z masses are all so much smaller than the Planck mass of order 10^{19} GeV, which is the only serious candidate we have for a fundamental mass scale in physics. In the Standard Model it is believed that the source of particle masses is a Higgs boson with mass $\leq$ 1 TeV [5], and the searches for this are discussed by the Physics-1 Working Group [6]. There is a general theoretical consensus that an elementary Higgs boson by itself has

insuperable technical problems, which can only be resolved by making the Higgs boson composite (the technicolour idea not discussed here) or else by protecting the Higgs with supersymmetry. Supersymmetric theories predict a large number of new particles which should all weigh $\leq$ 1 TeV if they are to do their job of stabilizing the mass of the Higgs boson [7]. Accordingly, supersymmetry suggests a rich domain of new physics at the next generation of accelerators. We discuss this extensively in the following.

The above list of problems is not exhaustive, but they and all other problems are by definition resolved in the Theory of Everything (TOE). In addition to solving the Unification, Flavour, and Mass Problems mentioned above, the TOE should also include gravity and reconcile it with quantum mechanics. It should probably be finite, may explain the origin of space and time, etc. The first serious candidate for such a TOE is the superstring [8]. It is, unfortunately, even further removed from everyday energies than are the GUTs mentioned above, and its predictions for current and forthcoming experiments are correspondingly even more ambiguous. Nevertheless, some preliminary attempts to relate the superstring to experiments have suggested the possible existence of one or more additional neutral Z′ bosons, and/or additional matter particles which might have leptoquark signatures [9]. Such speculative possibilities are also studied in this report.

Having revealed our theoretical prejudices, we now state the detector characteristics which we have assumed in a consistent way for the different accelerators. We assume energy resolutions

$$\delta E/E = 10\%/\sqrt{E} + 1\% \quad \text{for } e/\gamma \qquad 50\%/\sqrt{E} + 5\% \quad \text{for hadrons} \tag{1.1}$$

or

$$\delta E/E = 15\%/\sqrt{E} + 2\% \quad \text{for } e/\gamma \qquad 35\%/\sqrt{E} + 2\% \quad \text{for hadrons}, \tag{1.2}$$

and momentum resolution

$$\delta p/p = 10^{-4}\, p \quad \text{for charged-particle tracking} \tag{1.3}$$

or

$$\delta p/p = 0.10 \quad \text{for muons passing through magnetized iron}. \tag{1.4}$$

The granularity of the detector is assumed to be

$$\delta\eta = \delta\phi = 0.03 \quad \text{for } e/\gamma, \qquad \delta\eta = \delta\phi = 0.06 \quad \text{for hadrons}. \tag{1.5}$$

The angular coverage for track detection and calorimetry is assumed to be

$$|\eta| < 5 \qquad \text{in pp collisions}, \tag{1.6a}$$

$$10^\circ < \theta < 170^\circ \qquad \text{in } e^+e^- \text{ collisions}, \tag{1.6b}$$

and a combination of the two [(1.6a) in the p beam direction, (1.6b) in the e beam direction] in ep collisions. We believe it may be possible to install luminosity monitors down to 2° in e^+e^- collisions; but this is not essential to our subsequent discussion, and an adequate measurement of the luminosity may be possible using only detectors in the angular range (1.6b). The above numbers (1.1) to (1.6) are to be regarded as default options which apply to all the subsequent analyses unless a different assumption is clearly stated.

Finally, we recall the accelerator energies and luminosities which we have assumed. For the Large Hadron Collider (LHC) pp option, we generally take E_{cm} = 17 TeV and $L = 10^{33}\ cm^{-2}\ s^{-1}$ corresponding to an integrated luminosity of $10^{40}\ cm^{-2} = 10\ fb^{-1}$ per year [10]. We also make some comments in the concluding section on the additional physics available if $L \geq 10^{34}\ cm^{-2}\ s^{-1}$. For the LHC ep option, we mainly consider E_{cm} = 1.4 TeV and $L = 10^{32}\ cm^{-2}\ s^{-1}$, corresponding to an integrated luminosity of $10^{39}\ cm^{-2} = 1\ fb^{-1}$ per year [10]. We also compare its capabilities with those made available by running at E_{cm} = 1.8 TeV and $L = 10^{31}\ cm^{-2}\ s^{-1}$, bearing in

mind that longitudinal electron or positron beam polarization is only likely to be available at the lower energy. In view of the small e^+e^- cross-sections discussed later, for the CERN Linear Collider (CLIC) with $E_{cm} = 1$ to 2 TeV, we assume $L = 10^{33} (E_{cm}/1\ \text{TeV})^2\ \text{cm}^{-2}\ \text{s}^{-1}$, corresponding to an integrated luminosity of $10 (E_{cm}/1\ \text{TeV})^2\ \text{fb}^{-1}$ per year [11]. In this case, we comment explicitly on the physics one loses if only $L = 10^{33}\ \text{cm}^{-2}\ \text{s}^{-1}$ is available at $E_{cm} = 2$ TeV.

2. PHYSICS MATRIX

In this section we go row by row through the matrix of subjects in Table 1, treating in parallel the capabilities of the different accelerators for each physics topic. The numbering of the subsections (sub-subsections) corresponds to the rows (elements) of the matrix.

2.1 Supersymmetry

The most important searches for supersymmetric particles have been conducted at the CERN $p\bar{p}$ Collider and in e^+e^- collisions. The former is more powerful in the search for strongly interacting sparticles, the squarks $\tilde{q}$ and gluinos $\tilde{g}$, whilst PETRA and PEP establish the cleanest lower limits on the masses of electroweakly interacting sparticles such as sleptons $\tilde{\ell}$ and winos $\widetilde{W}$. No definite lower limit from the $p\bar{p}$ Collider on $m_{\tilde{q}}$ or $m_{\tilde{g}}$ has yet been published, but indications are that the UA1 Collaboration can probably establish [12]

$$m_{\tilde{q}} \geq 65\ \text{GeV} \quad \text{and} \quad m_{\tilde{g}} \geq 55\ \text{GeV} \tag{2.1}$$

if one assumes that $\tilde{q} \to q\tilde{\gamma}$ and $\tilde{g} \to q\bar{q}\tilde{\gamma}$, respectively, with $m_{\tilde{\gamma}} \ll m_{\tilde{q}}, m_{\tilde{g}}$. The ensemble of the e^+e^- experiments establishes [13]

$$m_{\tilde{\ell}} \geq 20\ \text{GeV} \quad \text{and} \quad m_{\widetilde{W}} \geq 20\ \text{GeV}\,. \tag{2.2}$$

For a complete list of current limits, some of which are stronger but more model-dependent, see Ref. [13].

The above limits are likely to be significantly improved before the LHC or CLIC comes into operation. In the field of $p\bar{p}$ collisions, the FNAL Tevatron Collider should be able to reach [14]

$$m_{\tilde{q}},\ m_{\tilde{g}} \simeq 200\ \text{GeV}\,, \tag{2.3}$$

whilst LEP 200 should be able to reach [15]

$$m_{\tilde{\ell}},\ m_{\widetilde{W}} \simeq 90\ \text{GeV}\,. \tag{2.4}$$

Our task will be to see how far beyond the limits [Eqs. (2.3) and (2.4)] the LHC and/or CLIC could reach, remembering also that theory expects sparticle masses ≤ 1 TeV.

2.1.1 Supersymmetry in pp collisions

This sub-subsection first summarizes the results of a new analysis [16] of $\tilde{q}$ and $\tilde{g}$ production in pp collisions based on a Monte Carlo evaluation of the signals and backgrounds using ISAJET version 5.23, which includes initial- and final-state gluon bremsstrahlung and the underlying event [17]. These results are then compared with those of an on-going analysis [14] that applies a uniform analysis technique to $\tilde{q}$ and $\tilde{g}$ production at the CERN $p\bar{p}$ Collider, the FNAL Tevatron Collider, and the Superconducting Super Collider (SSC). Finally, we discuss the possibilities of looking for electroweak sparticles such as $\tilde{e}$ and $\widetilde{W}$ at the LHC [18].

In the first analysis, the reactions

$$\begin{array}{lll} pp \to \tilde{q}\bar{\tilde{q}} + X\,, & & pp \to \tilde{g}\tilde{g} + X \\ \quad\ \ \big\lfloor\!\!\to \bar{q} + \tilde{\gamma} & & \quad\ \ \big\lfloor\!\!\to q\bar{q}\tilde{\gamma} \\ \quad\ \ \big\lfloor\!\!\to q + \tilde{\gamma} & & \quad\ \ \big\lfloor\!\!\to q\bar{q}\tilde{\gamma} \end{array} \tag{2.5}$$

are studied, assuming $m_{\tilde{\gamma}} \ll m_{\tilde{q}}, m_{\tilde{g}}$, giving the signature of jets + missing transverse momentum p_T. The signatures are unaffected if the $\tilde{\gamma}$ is replaced by some other light neutral sparticle such as an $\tilde{H}$, and other studies [19] have indicated that the cross-sections for these signatures are not greatly reduced for massive photinos in the range $m_{\tilde{\gamma}} \leq 1/2(m_{\tilde{q}}$ or $m_{\tilde{g}})$. However, we have not studied the effects of $\tilde{q} \to q(\widetilde{W}, \widetilde{Z})$ or $\tilde{g} \to q\bar{q}(\widetilde{W}, \widetilde{Z})$ decays, which would tend to reduce the missing transverse energy $\not{E}_T$ signature [20]. The backgrounds we have evaluated include

i) QCD jets, which can give real $\not{E}_T$ due to heavy flavour c,b,t $\to q\ell\nu$ decays, or fake $\not{E}_T$ owing to detector effects;

ii) $(W \to \ell\nu) + X$ and $(Z \to \nu\bar{\nu}) + X$, which give real $\not{E}_T$; and

iii) WW, WZ, and ZZ + X events.

The first two sources of background have been studied quantitatively as discussed below. The third class of source seems to have a much smaller cross-section [21]: a quantitative study will be given elsewhere [16]. The jet-finding algorithm used was based on the one adopted by UA1 [22]: one takes an initiator cell with $E_T > 5$ GeV, and then adds to the jet other cells with $E_T > 0.5$ GeV if $\Delta R \equiv \sqrt{(\Delta\eta)^2 + (\Delta\phi)^2} < 1$. Figure 1a shows the distribution in true

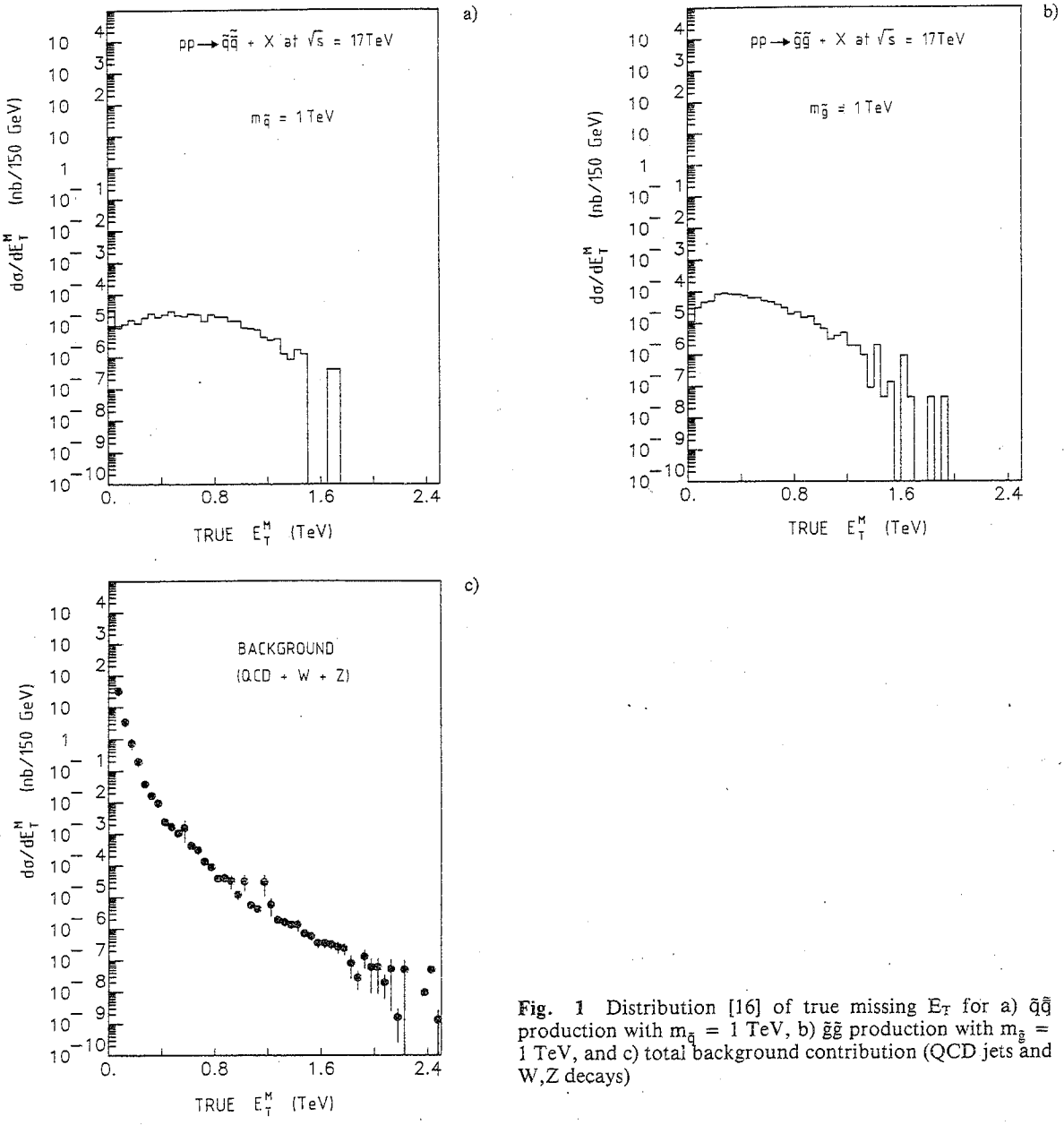

Fig. 1 Distribution [16] of true missing E_T for a) $\tilde{q}\tilde{q}$ production with $m_{\tilde{q}} = 1$ TeV, b) $\tilde{g}\tilde{g}$ production with $m_{\tilde{g}} = 1$ TeV, and c) total background contribution (QCD jets and W,Z decays)

$\not{E}_T$ due to ν and $\tilde{\gamma}$ from $\tilde{q}\bar{\tilde{q}}$ production with $m_{\tilde{q}} = 1$ TeV, assuming $m_{\tilde{g}} \gg m_{\tilde{q}}$. Figure 1b is the same for $\tilde{g}\tilde{g}$ production with $m_{\tilde{g}} = 1$ TeV assuming $m_{\tilde{g}} \ll m_{\tilde{q}}$, and Fig. 1c shows the true missing energy distribution from background sources (i) and (ii) above, assuming a top quark mass of 40 GeV (the backgrounds due to a heavier top quark or to fourth-generation quarks are discussed elsewhere [16]). We see that the signal and background distributions 'kiss' at $\not{E}_T \approx 0.8 m_{\tilde{q}}, m_{\tilde{g}}$, which is also true for smaller values of $m_{\tilde{q}}, m_{\tilde{g}}$.

As can be seen in Figs. 2a and 2b, the signal distributions are not greatly affected by detector smearing, whilst the steeply falling background distribution of Fig. 1c is significantly broadened by the detector as seen in Fig. 2c, resulting in a signal-to-background ratio of 1 to 5 or 10.

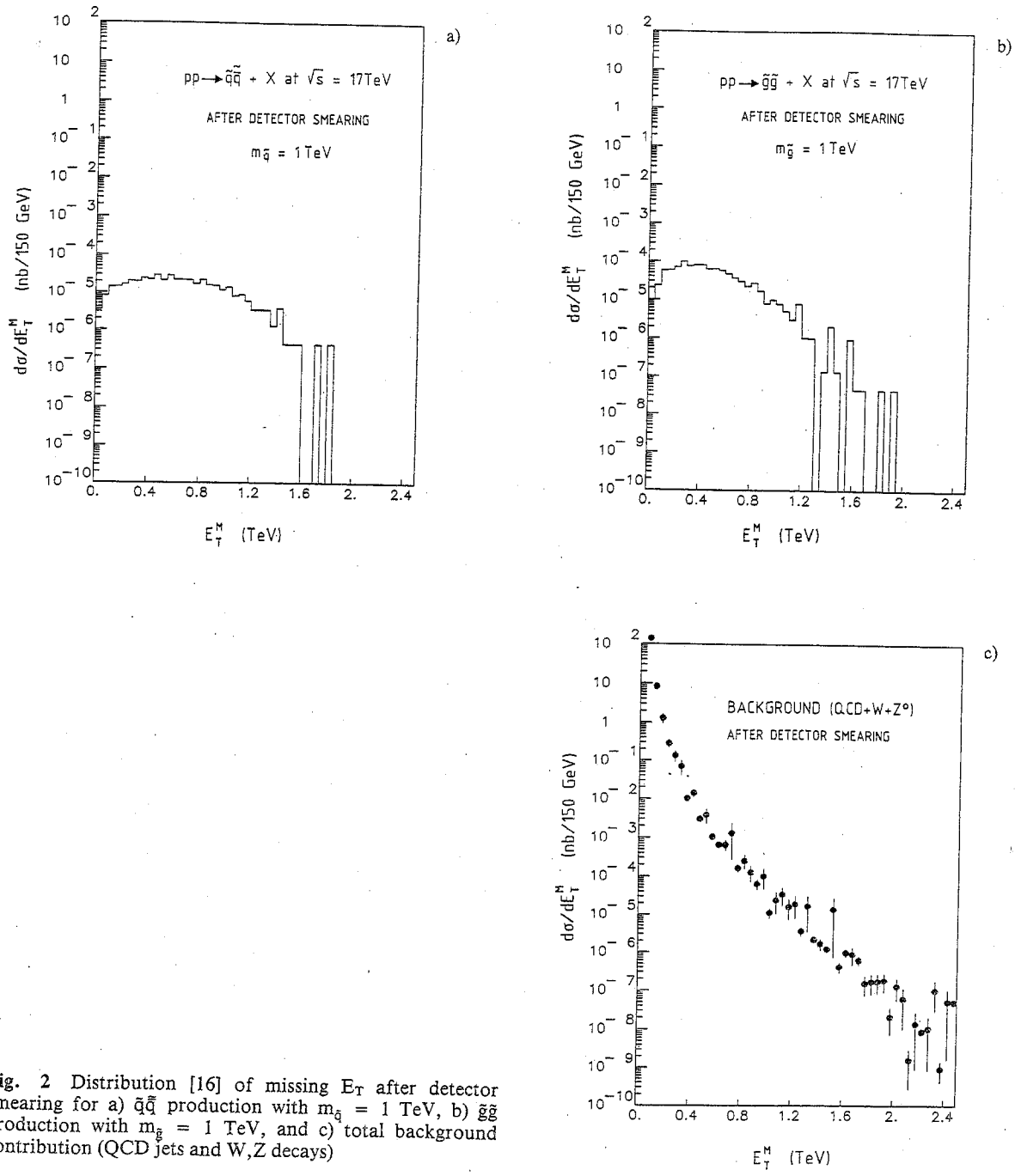

Fig. 2 Distribution [16] of missing E_T after detector smearing for a) $\tilde{q}\bar{\tilde{q}}$ production with $m_{\tilde{q}} = 1$ TeV, b) $\tilde{g}\tilde{g}$ production with $m_{\tilde{g}} = 1$ TeV, and c) total background contribution (QCD jets and W,Z decays)

Possible ways to reduce the background include the following:

i) A cut in $\not{E}_T$. We find that $\not{E}_T \geq 2/3 m_{\tilde{q}}$ or $m_{\tilde{g}}$ is the most sensitive domain.

ii) Remove events with an identified e or μ. (It might also prove possible to remove taus with some efficiency, but a detailed understanding of jet shape and charged multiplicity distribution would be required.) The lepton veto is necessary to reduce $W \to \ell\nu$ and semileptonic heavy-flavour decay backgrounds, although it does remove some of the sparticle events. Quantitatively, we have rejected events with p_T (e or μ) > 30 GeV in $|\eta| < 5$, and $\Sigma p_T < 5$ GeV in a cone of $\Delta R < 0.4$ about an electron.

iii) Cuts in event topology. These are based on the observations that $\tilde{q}\bar{\tilde{q}}$ events give mainly dijets + $\not{E}_T$ final states, where the jets are not back-to-back and the $\not{E}_T$ vector is isolated in azimuthal angle, and $\tilde{g}\tilde{g}$ events typically give multijet, quasi-isotropic final states, whilst QCD typically gives back-to-back dijet events with the $\not{E}_T$ vector aligned with the jet axes, apart from QCD radiative corrections.

iv) A top quark tag. This may be possible using, for example, a vertex detector and making a cut in apparent impact parameter. Such a tag would be very useful, because after the above cuts 1% of the background is due to b and c jets, O(1/3) is due to the $t\bar{t}$ jet-pair production, and O(2/3) is due to gluon jets splitting into $t\bar{t}$ pairs. (These numbers are for $m_t = 40$ GeV, and are expected to diminish for the case of larger m_t, which is studied elsewhere [16].)

As examples of possible topological cuts, Fig. 3a shows the distribution in azimuthal angle difference $\Delta\phi(\not{E}_T$, jet 1) and the cut $\Delta\phi < 130°$ which is used subsequently in the $\tilde{q}\bar{\tilde{q}}$ analysis, and Fig. 3b shows the distribution in circularity

$$C \equiv 1/2 \min (\Sigma p_T \cdot n)^2/(\Sigma p_T^2) \tag{2.6}$$

and the cut $C > 0.25$ which is used subsequently in the $\tilde{g}\tilde{g}$ analysis. Finally, Fig. 3c shows the distribution in the multiplicities of calorimeter jets with $E_T^{jet} > 250$ GeV for the $\tilde{q}\bar{\tilde{q}}$ case, and Fig. 3d shows the same distribution for the $\tilde{g}\tilde{g}$ case. We use a cut on jet multiplicity to separate $\tilde{q}\bar{\tilde{q}}$ candidates ($N_{jet} \leq 2$) and $\tilde{g}\tilde{g}$ candidates ($N_{jet} \geq 3$).

The results of applying these cuts are shown in Fig. 4a for the $\tilde{q}\bar{\tilde{q}}$ signal and for the backgrounds, which in this case are mainly W and Z events. The corresponding graphs for $\tilde{g}\tilde{g}$ events and their backgrounds are shown in Fig. 4b: in this case most of the backgrounds are QCD jets.

In Table 2 we show the expected event rates in a 10 fb^{-1} run for squarks and gluinos of different masses, and the different backgrounds for the two sets of cuts. We see that the signals exceed the backgrounds for lower values of $m_{\tilde{q}}$ and $m_{\tilde{g}}$, falling to a ratio of one-to-one for

$$m_{\tilde{q}} \approx 1 \text{ TeV}, \qquad m_{\tilde{g}} \approx 1 \text{ TeV}, \tag{2.7}$$

which are plausible values to quote as a discovery limit [16]. In the case of $\tilde{q}\bar{\tilde{q}}$ production, the dominant W background could perhaps be reduced by improving the lepton cuts which are not optimized. In the case of $\tilde{g}\tilde{g}$ production, the dominant QCD jet background could perhaps be reduced by the t quark tag mentioned earlier. In view of these possible improvements, we regard the limits (2.7) as being quite conservative. Nevertheless, the search for sparticles in pp collisions is a delicate affair, and would require a good understanding of (a) the Standard Model physics contributions and (b) the detector response to leptons and jets. Therefore we are fortunate to be able to compare two distinct analyses.

A uniform approach has been developed over a period of time and applied to squark and gluino searches at the CERN $p\bar{p}$ Collider, the FNAL Tevatron Collider, the LHC, and the SSC [14]. This analysis uses ISAJET version 5.25 to generate the three processes $pp \to \tilde{g}\tilde{g}$, $\tilde{g}\tilde{q}$, $\tilde{q}\bar{\tilde{q}}$ + X, and simulates a 4π fine-grain calorimeter. A simple cluster algorithm is used, which looks for the highest E_T cell above 2 GeV, includes all nearest-neighbour cells above 500 MeV, and also determines if two or more clusters touch. Clusters whose centres have $\Delta R = \sqrt{(\Delta\eta)^2 + (\Delta\phi)^2} < 1$ are merged and called jets if their $E_T > 20$ GeV.

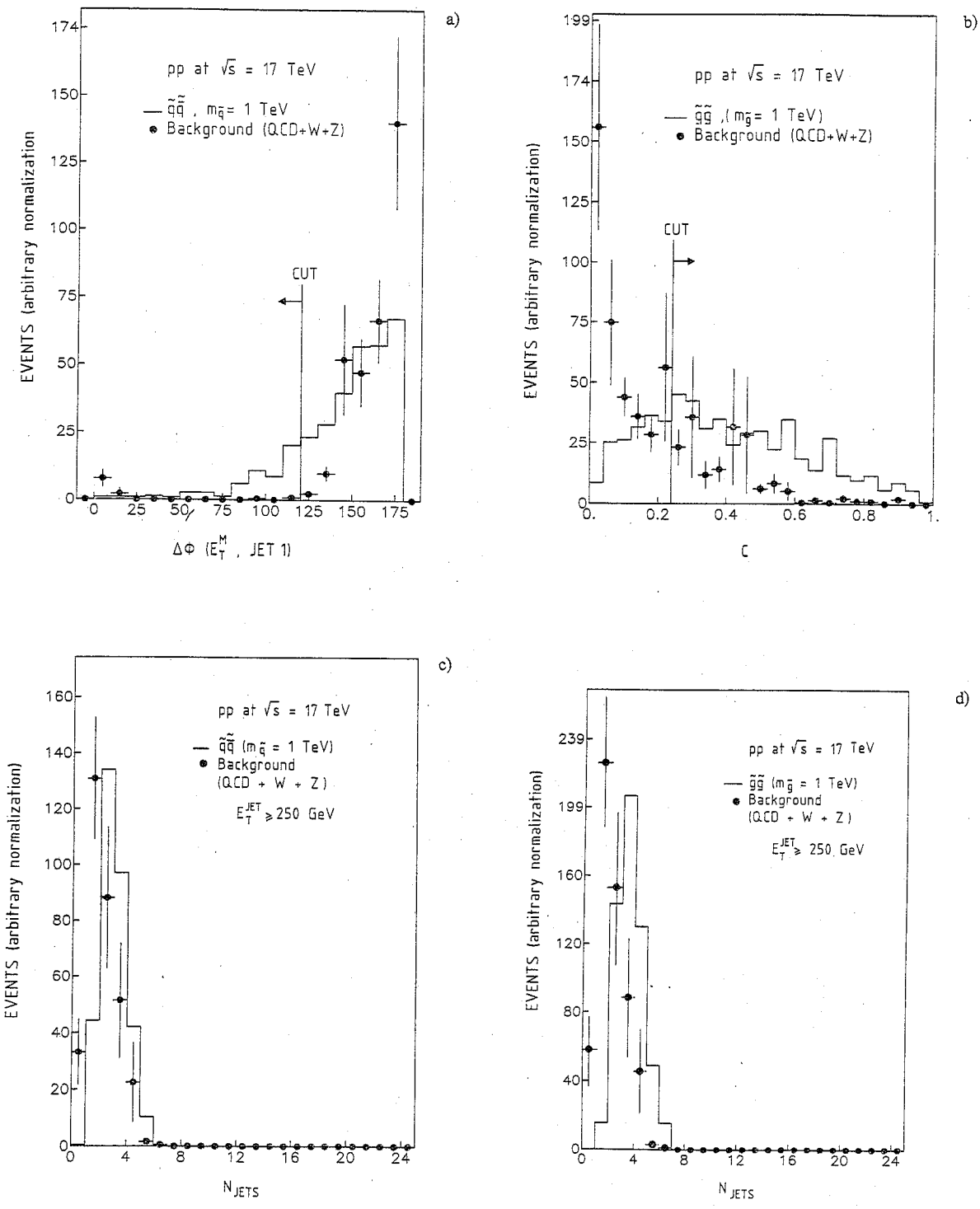

Fig. 3 Distributions [16] of a) azimuthal angle difference $\Delta\phi$ between highest jet E_T and missing E_T for $\tilde{q}\bar{\tilde{q}}$ ($m_{\tilde{q}}$ = 1 TeV) and total background, b) circularity for $\tilde{g}\tilde{g}$ ($m_{\tilde{g}}$ = 1 TeV) and total background; calorimeter jet multiplicity, c) for the total background and $\tilde{q}\bar{\tilde{q}}$ ($m_{\tilde{q}}$ = 1 TeV), d) for the total background and $\tilde{g}\tilde{g}$ ($m_{\tilde{g}}$ = 1 TeV). Only events with $\not{E}_T > 300$ GeV are included.

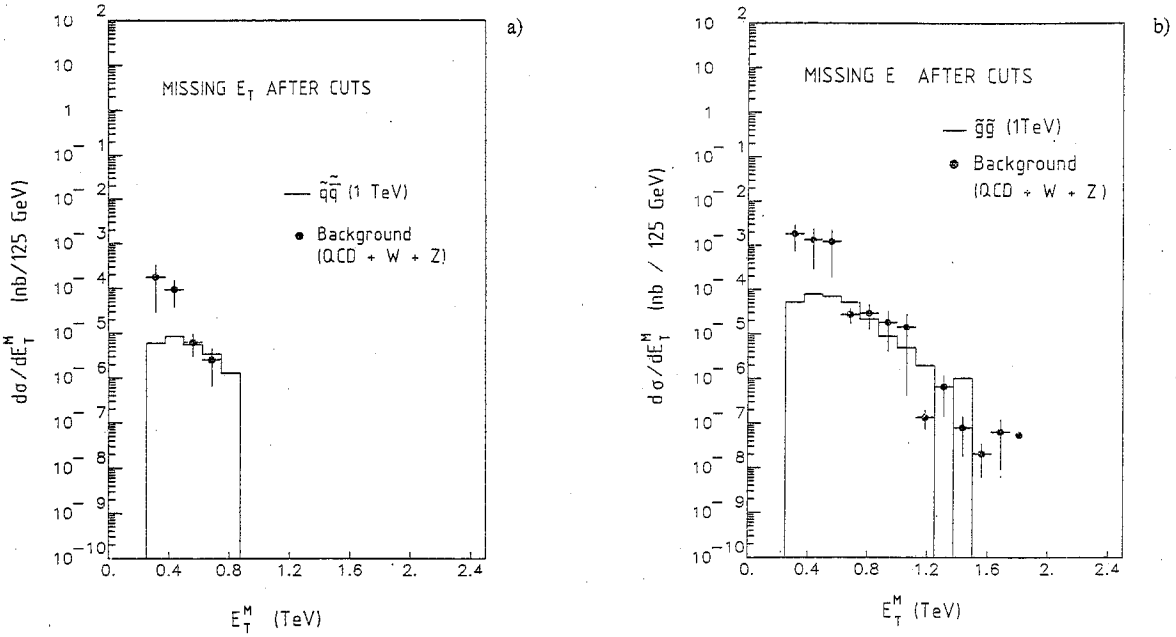

Fig. 4 Missing-E_T distribution [16] after all cuts a) for $\tilde{q}\bar{\tilde{q}}$ ($m_{\tilde{q}}$ = 1 TeV) and total background predictions, b) for $\tilde{g}\tilde{g}$ ($m_{\tilde{g}}$ = 1 TeV) and total background events, after the cuts described in the text

Table 2

Expected events rates [16] in a 10 fb^{-1} run for squarks, gluinos, and background contributions, computed from the ISAJET Monte Carlo version 5.23. The errors quoted are the statistical ones from the Monte Carlo generation.

	$N_{jet} \geq 3$, $C > 0.25$		$N_{jet} \leq 2$, $\Delta\phi < 130°$	
	$\not{E}_T > 600$ GeV	$\not{E}_T > 800$ GeV	$\not{E}_T > 600$ GeV	$\not{E}_T > 800$ GeV
QCD	940 ± 300	320 ± 200	0	0
$W \rightarrow \ell\nu$	130 ± 45	30 ± 19	18 ± 5.1	0
$Z \rightarrow \nu\nu$	26 ± 8.8	7.3 ± 3.6	7.2 ± 5.1	0
ΣBGD	1096 ± 303	357 ± 201	25.2 ± 19	0
Sparticle masses	Gluinos		Squarks	
2000 GeV	11 ± 0.6	7.4 ± 0.5	5.8 ± 0.8	3.8 ± 0.7
1500 GeV	100 ± 6.5	53 ± 4.7	21 ± 3.3	9.8 ± 2.3
1000 GeV	1000 ± 100	300 ± 53	64 ± 17	4.3 ± 4.3
800 GeV	2200 ± 290	520 ± 140	160 ± 47	14 ± 14
600 GeV	4000 ± 960	700 ± 410	660 ± 210	

The ranges of sparticle masses studied in [14] have been restricted to those expected in a Minimal Supersymmetric Standard Model (MSSM), in which the gluino may only be slightly heavier than the squark—in which case $\tilde{g} \to \tilde{q}\bar{q}$ and $\tilde{q} \to q\tilde{\gamma}$, or $m_{\tilde{g}} < m_{\tilde{q}}$—in which case $\tilde{g} \to q\bar{q}\tilde{\gamma}$ and $\tilde{q} \to q\tilde{g}$, or $m_{\tilde{g}} \ll m_{\tilde{q}}$—in which case $\tilde{g} \to q\bar{q}\tilde{\gamma}$ and we restricted ourselves to the $\tilde{q} \to q\tilde{\gamma}$ decays which have a branching ratio of a few percent. Most of the resulting final states at the Tevatron and higher energies have ≥ 3 jets with $\not{p}_T$, and the main Standard Model background is due to QCD jets containing light or heavy quarks. A detailed quantitative study [14] of this background indicates that for large E_T jets it closely resembles the supersymmetric signal, and that a cut in $\not{p}_T$ alone is not sufficient in most of the cases considered, as seen in Table 3. Therefore we make cuts on the event topology using the variables

$$x_E = \frac{\not{p}_T \cdot \underline{e}_1}{E_T^{tot}}, \qquad x_{out} = \frac{|\not{p}_T \times \underline{e}_1|}{E_T^{tot}} \tag{2.8}$$

where $\underline{e}_1$ is a unit vector along the direction of the highest E_T jet, or (almost equivalently) the sphericity axis. This is sufficient to detach the signal from the background, as seen for the x_{out} variable in Fig. 5. Details of the effects of these cuts on the signal-to-background ratios for various choices of $m_{\tilde{q}}$ and $m_{\tilde{g}}$ are shown in Table 3. More details, including a comparison of the Tevatron Collider with $\int L\,dt = 10^{36}\ cm^{-2}\ s^{-1}$ or $10^{39}\ cm^{-2}\ s^{-1}$, the LHC at $\sqrt{s} = 17$ TeV and the SSC at $\sqrt{s} = 40$ TeV with $\int L\,dt = 10^{40}\ cm^{-2}\ s^{-1}$, and choices of $m_{\tilde{q}}$ and $m_{\tilde{g}}$ from < 100 GeV to 1.5 TeV are given in Ref. [14].

The main conclusions of this analysis are as follows:

1) The Tevatron will be able to reach $m_{\tilde{q}}, m_{\tilde{g}} \approx 100$ GeV when it achieves $\int L\,dt = 10^{36}\ cm^{-2}\ s^{-1}$, and $m_{\tilde{q}} \approx 350$ GeV, $m_{\tilde{g}} \approx 200$ GeV if it achieves $\int L\,dt = 10^{39}\ cm^{-2}\ s^{-1}$.
2) The LHC overlaps with the Tevatron for squarks and gluinos with masses between 200 and 400 GeV.
3) The rate at the LHC with 10 fb^{-1} varies from about 2×10^7 events for $m_{\tilde{q}} \approx m_{\tilde{g}} \approx 300$ GeV, compared with about 3×10^8 QCD background events, to about 2×10^4 events for $m_{\tilde{q}} \approx m_{\tilde{g}} \approx 1$ TeV, compared with about 2×10^7 QCD background events. After applying the proposed cuts, the signal-to-background ratio falls from 50 to 90 in the low-mass case, through about 10 to 20 when $m_{\tilde{q}} \approx m_{\tilde{g}} \approx 500$ GeV, to about 1 when $m_{\tilde{q}} \approx m_{\tilde{g}} \approx 1$ TeV. A bound of about 1 TeV seems to be attainable at the LHC with effort.
4) The SSC could reach out to sparticle masses ≈ 1.5 TeV.

It should be noted that neither of the above pp → squark, gluino analyses includes contributions from jet fluctuations, which could be important for light sparticle masses.

We conclude this subsection by reporting on an analysis [18] of pp → electroweak sparticles + X. The processes studied were

$$\begin{array}{lll} pp \to \tilde{\ell}^+\tilde{\ell}^- + X, & & pp \to \tilde{q} + \tilde{W} + X \\ \quad \big\lfloor \hookrightarrow e^- + \tilde{\gamma} & & \quad \big\lfloor \hookrightarrow e\nu\tilde{\gamma} \\ \quad \hookrightarrow e^+ + \tilde{\gamma} & & \quad \hookrightarrow q\tilde{\gamma} \end{array} \tag{2.9}$$

For the first process, the backgrounds studied were

i) Drell-Yan: $pp \to (\gamma, Z \to e^+e^-) + X$, which can be removed by simple cuts $m_{e^+e^-} > 200$ GeV and $\not{E}_T > 40$ GeV, and

ii) $pp \to (W^- \to e^-\nu) + (W^+ \to e^+\nu) + X$, which can be removed by strengthening the $\not{E}_T$ cut to $\not{E}_T > 100$ GeV.

After these cuts one could see

$$m_{\tilde{e}} \approx 300\ \text{GeV}, \tag{2.10}$$

under the traditional assumptions $m_{\tilde{W}} \gg m_{\tilde{e}} \gg m_{\tilde{\gamma}}$ [18]. However, these assumptions are not necessarily valid in realistic supersymmetric models based on supergravity theories [7], and the changes in the spectra have a significant effect on the bound (2.10). In minimal models of the supergravity type, the physical sparticle masses are given in terms of two bare mass parameters $(m_0, m_{1/2})$ by

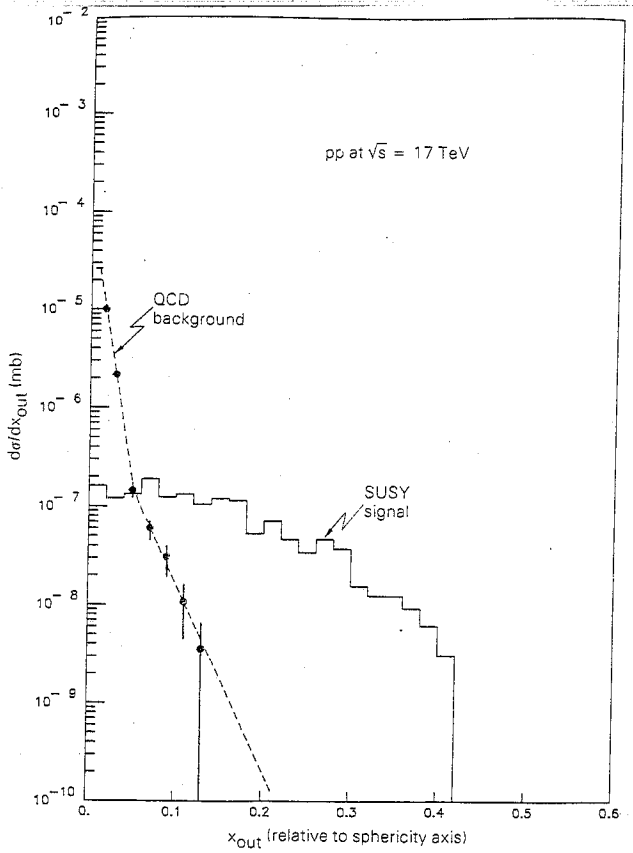

Fig. 5 Distribution in $d\sigma/dx_{out}$ for the process $pp \to \tilde{g}\tilde{q}$ assuming $m_{\tilde{g}} = 315$ GeV, $m_{\tilde{q}} = 285$ GeV and the decay modes $\tilde{g} \to q\bar{q}\tilde{\gamma}$, $\tilde{q} \to q\tilde{\gamma}$ at $\sqrt{s} = 17$ TeV (full line), compared with one obtained for the corresponding QCD background (i.e. where the QCD jets are required to have $p_T > 300$ GeV). A fit to the QCD background (dashed line) has been made so as to estimate the tail of this background.

Table 3

Comparison [14] of supersymmetry signal and QCD background for pp collisions at $E_{cm} = 17$ TeV. The supersymmetry signal includes all three processes $pp \to \tilde{g}\tilde{g}$, $\tilde{g}\tilde{q}$ and $\tilde{q}\tilde{q}$.

Sparticle masses (GeV)		σ (mb)	Signal/background ratio (% of signal retained)			
$m_{\tilde{g}}$	$m_{\tilde{q}}$		No cut	$\not{E}_T > 200$ GeV	$x_E > 0.24$	$x_{out} > 0.08$
210	483	0.59×10^{-5}	0.21	13 (7.6%)	8.7 (6%)	94 (29%)
315	285	1.84×10^{-6}	0.06	21 (42%)	14 (31%)	58 (50%)
350	805	0.47×10^{-6}	0.21	5 (27%)	4 (11%)	17 (32%)
525	475	1.3×10^{-7}	0.06	3.3 (63%)	4.2 (41%)	9 (54%)
700	1610	0.74×10^{-8}	3.4×10^{-3}	0.27 (65%)	0.1 (12%)	0.54 (40%)
1050	950	1.92×10^{-7}	8.4×10^{-2}	0.75 (80%)	0.1 (52%)	0.2 (68%)

For more details of the QCD background evaluation, see [14].

$$m_{\tilde{q}}^2 \simeq m_0^2 + 7m_{1/2}^2 , \qquad m_{\tilde{l}_{L,R}}^2 \simeq m_0^2 + (0.5, 0.15)m_{1/2}^2 ,$$
$$m_{\tilde{g}} \simeq 3m_{1/2} , \qquad m_{\tilde{\gamma}} \simeq 0.47m_{1/2} , \qquad m_{\tilde{W}} \simeq 0.84m_{1/2} . \tag{2.11}$$

The domain of the $(m_0, m_{1/2})$ parameter plane which can be excluded by the search for $pp \rightarrow \tilde{e}^+\tilde{e}^- + X$ is shown in Fig. 6: it only extends out to $m_{\tilde{e}} \approx 200$ GeV if $m_{1/2} = 0$ [18]. For the second process in (2.9), the main background considered has been $pp \rightarrow (W \rightarrow e\nu) + \text{jets} + X$. This can be removed by cutting on $m_T(e, \not{E}_T) > 150$ GeV, after which one has sensitivity to

$$m_{\tilde{W}} \approx 450 \text{ GeV} \tag{2.12}$$

if $m_{\tilde{W}} = m_{\tilde{q}} \gg m_{\tilde{\gamma}}$[18]. Again, the precise value of the reach (2.12) depends on the ratios of sparticle masses assumed, and the accessible domain of the $(m_0, m_{1/2})$ plane in the minimal supergravity model (2.11) is also shown in Fig. 6. This will be compared later with the capabilities of other present and future accelerators.

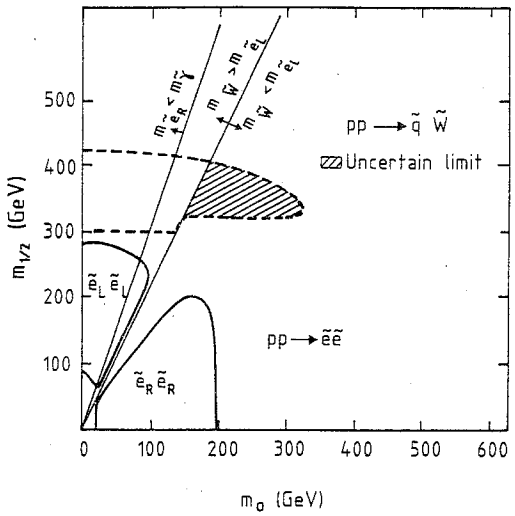

Fig. 6 Discovery limits [18] in the $(m_0, m_{1/2})$ plane for electroweak sparticle production in pp collisions at $\sqrt{s}$ = 17 TeV

2.1.2 Supersymmetry in ep collisions

The following sparticle production processes in ep collisions have been considered [23]:

$$ep \rightarrow \tilde{e}\tilde{q} + X , \tilde{\nu}\tilde{q} + X , \tilde{e}\tilde{\gamma} + X, \tilde{\nu}\tilde{W} + X, e\tilde{g}\tilde{q} + X , e\tilde{q}\tilde{q} + X . \tag{2.13}$$

The first two processes have the largest cross-sections and are the only ones discussed here. These final states are produced by gaugino and shiggs exchanges in the crossed channel: $\tilde{\gamma}/\tilde{Z}/\tilde{H}^0_{1,2}$ exchange in the case of the $\tilde{e}\tilde{q}$ final state, and $\tilde{W}^{\pm}/\tilde{H}^{\pm}$ exchange in the case of the $\nu\tilde{q}$ final state. The model for gaugino and shiggs mixing can be specified up to a possible discrete ambiguity by two masses, which we take to be the lightest neutral state and the lightest charged state, which we call the $\tilde{\gamma}$ and $\tilde{W}^{\pm}$, respectively, although these are not pure states.

As can be seen in Fig. 7, the cross-sections are quite sensitive to the chosen values of $m_{\tilde{\gamma}}$ and $m_{\tilde{W}}$ [24]. Taking as our detection limit a cross-section of 10^{-37} cm^2 corresponding to 10 (100) events per year at a luminosity of 10^{31} (10^{32}) cm^{-2} s^{-1}, and adding together the $\tilde{e}\tilde{q}$ and $\tilde{\nu}\tilde{q}$ processes, we find that the following sparticle masses can be reached [23]:

$$\text{equal mass:} \qquad m_{\tilde{e}} = m_{\tilde{q}} \approx 350 \text{ GeV} ,$$
$$\text{unequal mass:} \quad m_{\tilde{q}} \approx 700 \text{ GeV} , \text{ if } m_{\tilde{e}} = 50 \text{ GeV} . \tag{2.14}$$

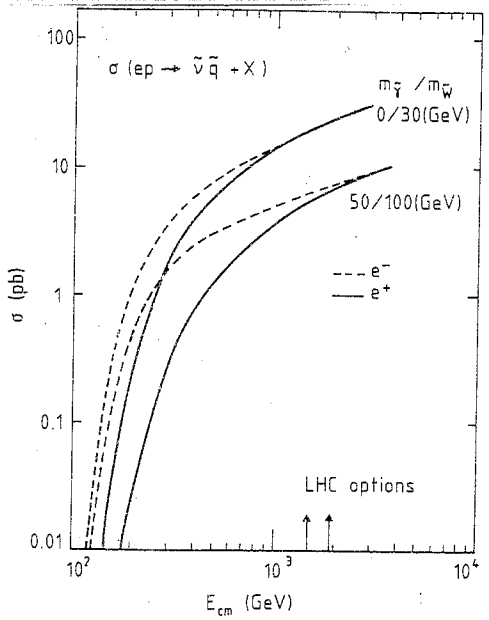

Fig. 7 Cross-section $\sigma(ep \to \tilde{\nu}\tilde{q} + X)$ as a function of $\sqrt{s}$ [23]. Assumed mass values for $\tilde{\nu}$ and $\tilde{q}$ are 50 GeV. The two sets of curves represent different choices of $m_{\tilde{\gamma}}$ and $m_{\tilde{W}}$.

We have not made an extensive study of all the possible backgrounds, since no ep event generator analogous to ISAJET is yet available. A careful study of heavy-flavour backgrounds such as $ep \to et\bar{t} + X$, $\nu t\bar{b} + X$ is desirable. We have considered the possible backgrounds from conventional neutral- and charged-current events. In the case of neutral-current events, one can measure the kinematic variables x and y in two independent ways, using either the outgoing e or the outgoing hadronic jet, and also measure their azimuthal angles. In usual neutral-current events $x_e = x_j$, $y_e = y_j$, and $\phi_e = \phi_j + \pi$; but in $(\tilde{e} \to e\tilde{\gamma})(\tilde{q} \to q\tilde{\gamma})$ events, $\Delta x \equiv x_e - x_j$, $\Delta y \equiv y_e - y_j$, and $\Delta\phi \equiv \phi_e - \phi_j - \pi$ are all non-zero in general. Previous HERA studies [25] have shown that the neutral-current background can easily be removed with cuts $|\Delta y| > 0.2$ and $|\Delta\phi| > 0.2$, which reduces the signal by at most 20%. We believe that similar arguments can be extended to the LHC ep option, and hence that the limits (2.14) are reasonably conservative.

2.1.3 Supersymmetry in e^+e^- collisions

An essential fact to remember is that all e^+e^- annihilation cross-sections are small [26]. It is useful to take as a standard of comparison the QED cross-section for $e^+e^- \to \mu^+\mu^-$:

$$\sigma \equiv \sigma(e^+e^- \to \gamma^* \to \mu^+\mu^-) = 4\pi\alpha^2/3E_{cm}^2 = 87\ \text{fb}/[E_{cm}\,(\text{TeV})]^2 \qquad (2.15)$$

which gives 220 $\mu^+\mu^-$ pairs per year at $E_{cm} = 2$ TeV, in the canonical year of 10^7 s at $L = 10^{33}\ \text{cm}^{-2}\,\text{s}^{-1}$. Other annihilation cross-sections, e.g. $e^+e^- \to q\bar{q}$, may be rather larger than (2.15), but many interesting sparticle pair-production cross-sections are actually significantly smaller than (2.15). For pair-production of a generic spin-0 pair $s\bar{s}$,

$$R \equiv \frac{\sigma(e^+e^- \to \gamma^* \to s\bar{s})}{\sigma(e^+e^- \to \gamma^* \to \mu^+\mu^-)} = 1/4Q_s^2N_c\beta^3\,, \qquad \beta \equiv p/E\,, \qquad (2.16)$$

where Q_s is the charge of s, and N_c is the number of colours it has (one for sleptons, three for squarks). Using Eq. (2.16), one has $R_{\tilde{\mu}} = 1/4\beta^3$, $R_{D_0} = 1/12\beta^3$ (where D_0 is the charge-1/3 colour triplet scalar discussed in

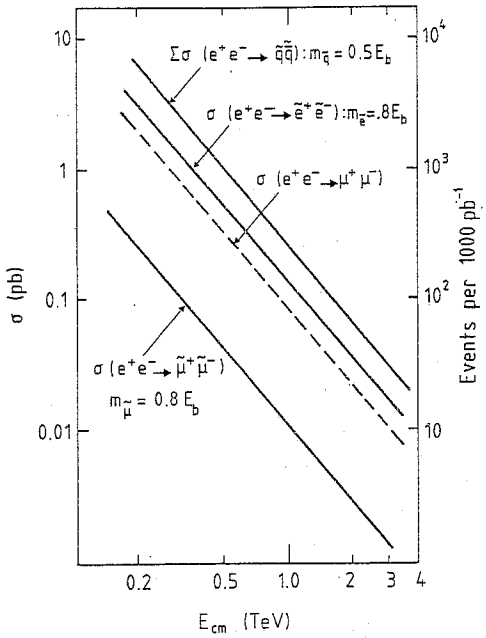

Fig. 8 Typical cross-sections [27] for $e^+e^- \rightarrow$ sparticles and $\rightarrow \mu^+\mu^-$ as functions of E_{cm}

sub-subsection 2.3.3) and $\beta^3 = 0.65$ (0.22) for $m/E_{beam} = 0.5$ (0.8). Figure 8 shows a compilation [27] of typical supersymmetry cross-sections as a function of E_{cm}, including Z^*as well as γ^* exchange. To do some reasonable physics, we need about 10^3 $\mu^+\mu^-$ pairs per year, corresponding to

$$L = 10^{33} (E_{cm}/1\ \text{TeV})^2\ \text{cm}^{-2}\ \text{s}^{-1}, \tag{2.17}$$

which means $L = 4 \times 10^{33}\ \text{cm}^{-2}\ \text{s}^{-1}$ at $E_{cm} = 2$ TeV. The implications for physics if the target (2.17) is not reached are discussed in the Conclusions (Section 3).

Many Monte Carlo studies of the search for supersymmetry have been made for planned e^+e^- machines at high centre-of-mass energies, such as LEP 100 and 200. Based on these studies, we tried to estimate the detector and machine requirements for a very high e^+e^- linear collider in the TeV range. The goal was to see how far the energy range could be explored and investigated. As discussed below, our selection criteria are optimized for sparticle masses in the region of (0.3 to 1) times the beam energy, with emphasis on the high mass range.

The characteristic signature of supersymmetric particle pair-production is events with missing energy, missing transverse momentum and total momentum, and dijet or dilepton final states which are acollinear and acoplanar. The subsequent analysis [27] emphasizes the use of missing transverse momentum and acoplanarity, which is insensitive to any longitudinal momentum imbalance occasioned by beamstrahlung. For the CLIC parameters [11] studied, the amount of this imbalance does not, in fact, seem large enough to be troublesome. We will discuss three sparticle searches in some detail: those for $\tilde{\mu}^+\tilde{\mu}^-$, $\tilde{e}^+\tilde{e}^-$, and $\tilde{W}^+\tilde{W}^-$.

1) $e^+e^- \rightarrow \tilde{\mu}^+\tilde{\mu}^-$

We select events with a $\mu^+\mu^-$ pair in which each μ is well contained in the detector with $|\cos\theta| < 0.87$ ($\theta < 30°$) and has an energy of more than 30 GeV. The background sources considered which can give two muons in the final state are $e^+e^- \rightarrow \mu\mu(\gamma)$, $\tau\tau(\gamma)$ with both taus decaying to $\mu\nu\nu$ (4% of the total $\tau^+\tau^-$ cross-section), and W^+W^- pairs with both W's decaying to $\mu\nu$ (< 1% of the total W^+W^- cross-section). The μ's from $\mu\mu(\gamma)$ and $\tau\tau(\gamma)$ are either back-to-back in the plane transverse to the beam, or have a high-energy γ within the detector acceptance. Because of the high energy of the W (1 TeV) compared to its mass, the μ's from W's are also almost back-to-back in the plane transverse to the beam, and in addition are sharply forward peaked. The distributions of $\tilde{\mu}\tilde{\mu}$, $\mu\mu(\gamma)$, and

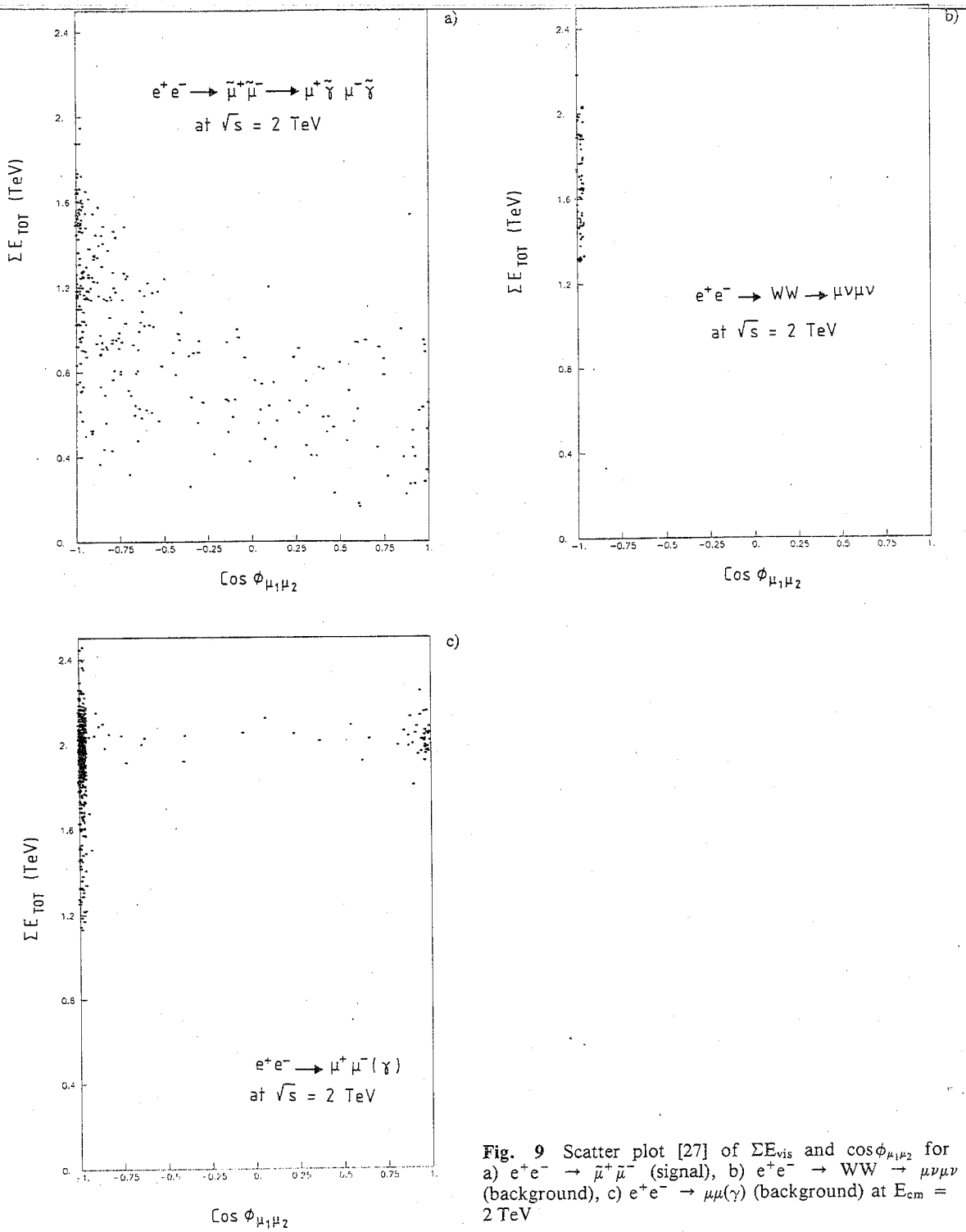

Fig. 9 Scatter plot [27] of ΣE_{vis} and $\cos\phi_{\mu_1\mu_2}$ for a) $e^+e^- \rightarrow \tilde{\mu}^+\tilde{\mu}^-$ (signal), b) $e^+e^- \rightarrow WW \rightarrow \mu\nu\mu\nu$ (background), c) $e^+e^- \rightarrow \mu\mu(\gamma)$ (background) at E_{cm} = 2 TeV

WW ($\rightarrow \mu\mu\nu\nu$) events in the (ΣE_{vis}, $\cos\phi_{\mu_1\mu_2}$) plane are shown in Fig. 9. There is a clear separation between the signal and the considered backgrounds. A signal with negligible background can be obtained by requiring that the angle $\phi_{\mu_1\mu_2}$ between the two μ's fulfil $\cos\phi_{\mu_1\mu_2} > -0.9$ and that the total visible energy be $< 0.9E_{cm}$.

The acceptance is of the order of 50–60% for masses above half the beam energy. Figure 10 shows the accepted cross-section with the cuts described above. From this we conclude that with 10 fb^{-1} integrated

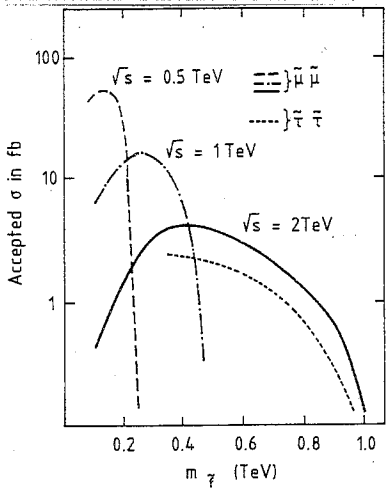

Fig. 10 Accepted $\tilde{\mu}^+\tilde{\mu}^-$ and $\tilde{\tau}^+\tilde{\tau}^-$ cross-sections [27] in e^+e^- collisions as functions of $m_{\tilde{l}}$ for different energies

luminosity, a clean signal can be detected up to masses of 800 GeV. An integrated luminosity of 50 fb^{-1} would allow this range to be extended up to

$$m_{\tilde{\mu}} \approx 850\text{–}900 \text{ GeV} . \tag{2.18}$$

This luminosity would also allow detailed studies with the detected events, as will be described below.

2) $e^+e^- \to \tilde{e}^+\tilde{e}^-$

Because of the t-channel photino exchange the cross-section is larger, as shown as the solid line in Fig. 11a. The signal can be isolated by selecting electron pairs with $\not{p}_T > 125$ GeV. This cut gets rid of most of the QED background such as eeγ. The events from WW $\to e\nu e\nu$ and $e\nu\tau\nu$ (where $\tau \to e\nu\nu$) have a product of cross-section and branching ratio of $\approx$ 0.007 pb, which after the p_T cut goes to 0.001 pb. The dependence of the accepted electron-pair cross-section on the selectron mass for $m_{\tilde{\gamma}} = 40$ GeV and $m_{\tilde{Z}} = 1000$ GeV is shown as the dashed line in Fig. 11a. The selectron can easily be detected up to masses of 800 GeV with a luminosity of 10 fb^{-1}, and up to

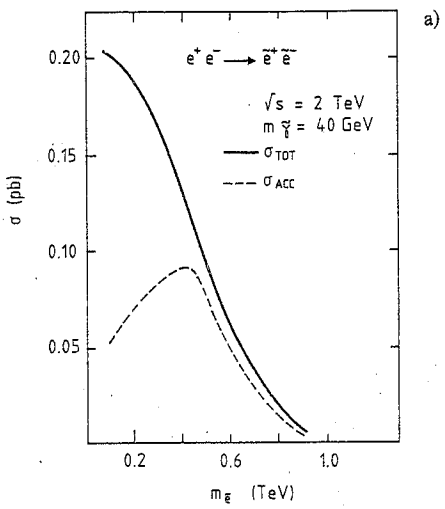

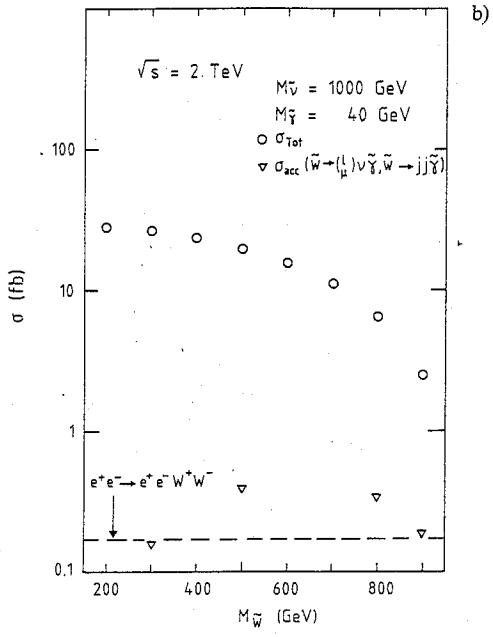

Fig. 11 Cross-sections [27] before and after selection cuts (see text) a) of $\tilde{e}^+\tilde{e}^-$ production as a function of slepton mass, and b) of wino production in e^+e^- collisions as a function of the wino mass

$$m_{\tilde{e}} \approx 900\ \text{GeV}\,. \qquad (2.19)$$

with an integrated luminosity of 50 fb^{-1} at E_{cm} = 2 TeV [27].

3) $e^+e^- \to \tilde{W}^+\tilde{W}^-$

The cross-section as a function of $m_{\tilde{W}}$ is shown in Fig. 11b. Here we base our analysis on the expected dominant decay mode $\tilde{W} \to \tilde{W}\tilde{\gamma}$, and investigate the final state where one W decays to an $e(\mu)\nu$ and the other to $q\bar{q} \to$ jets, corresponding to roughly 30% of the total $\tilde{W}^+\tilde{W}^-$ cross-section. Possible backgrounds for this could be W pair-production and the higher-order processes $e^+e^- \to e^+e^-W^+W^-$ or $e^+e^- \to e^\pm\nu + W^\pm Z^0$ followed by $W^\pm \to \ell^\pm\nu + Z^0 \to q\bar{q}$. Other new exotic particles such as a new heavy lepton or an extra W′ would give a signature similar to the expected signal; however, these backgrounds (being also a discovery) were not considered in the analysis described below. To obtain a signal we required the following selection criteria:

each parton (jet) should have an energy of more than 100 GeV;

Σ E(jets) $< 0.7E_{beam}$ (to eliminate the W^+W^- pair background);

$\cos\theta < 0.87$ (leptons) and < 0.94 (jets).

With these cuts we retain a visible cross-section of 1/10 of σ_{tot} for the $\tilde{W}$ signal.

Applying the same cuts to the Monte Carlo simulation of the reaction $e^+e^- \to e^+e^-W^+W^-$ and $e^+e^- \to e^\pm\nu W^\pm Z^0$ [21], the remaining background has a cross-section of roughly 10 fb. To remove it, one has to apply strong cuts, using the supersymmetry signature of missing transverse energy [$\not{E}_T > 200$ GeV] and acoplanarity angle ϕ [$\cos\phi$ (W-lepton) > -0.8]. With these cuts it is possible to reduce the background cross-section to below 0.2 fb, while keeping a signal cross-section of 0.38 fb ($m_{\tilde{W}}$ = 500 GeV) to 0.34 fb ($m_{\tilde{W}}$ = 800 GeV). Thus we conclude that a significant (about 5σ) signal of about 17 events above a background of < 10 events can be seen with an integrated luminosity of 50 fb^{-1} for

$$m_{\tilde{W}} \approx 850\ \text{GeV}\,. \qquad (2.20)$$

It should be kept in mind that we have assumed a pessimistic scenario for the branching ratios and the cross-section for $\tilde{W}^+\tilde{W}^-$ production. In addition, the significance could be increased by searching for a $\tilde{W}$ signal in the total hadronic final-state W decays.

Similar analyses of $e^+e^- \to \tilde{\tau}\tilde{\tau}$, and $\tilde{q}\bar{q}$ lead to analogous bounds on these sparticles [27].

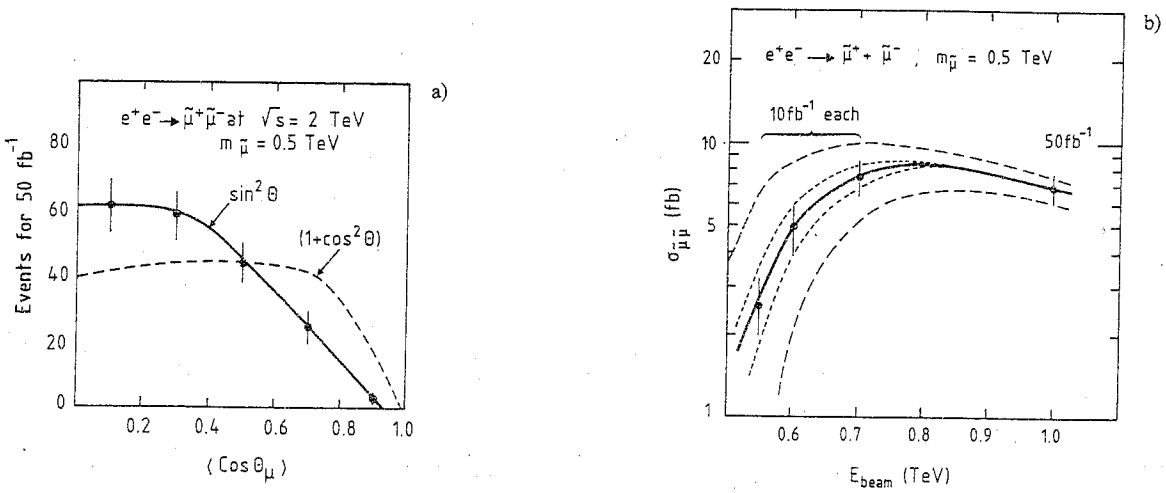

Fig. 12 a) Average angular distributions of muons at E_{cm} = 2 TeV. The solid line corresponds to a spin-0 smuon of mass 500 GeV, the dashed line to a spin-½ particle. b) Total cross-section as a function of beam energy. The solid (dashed) (dotted) lines correspond to smuons of mass 500 (±50) (±10) GeV. The bars represent the statistical errors in cross-section measurements with the indicated luminosities (see Ref. [27]).

It is important to note that the greater cleanliness of sparticle production in e^+e^- collisions compared with pp collisions allows one to verify the supersymmetric nature of the observed new phenomena, and also to investigate in detail the properties of the new particles. For example, the spin and the mass of the $\tilde{\mu}$ could be determined. Because they have spin 0, the $\tilde{\mu}$ are produced with $\sin^2\theta$ angular distributions, and there is a significant correlation between the angles of the parent $\tilde{\mu}$ and the daughter μ if $m_{\tilde{\mu}}/E_{cm}$ is small enough, which can be used to verify the spin of the $\tilde{\mu}$. Figure 12a shows the distribution in $\langle\cos\theta_\mu\rangle \equiv 1/2\,(\cos\theta_{\mu_1} - \cos\theta_{\mu_2})$ for $m_{\tilde{\mu}} = 500$ GeV at $E_{cm} = 2$ TeV, and the corresponding distribution that would be given by two-particle decay of a comparison particle of spin $^1/_2$. We find that with 190 events detected, it would be possible to distinguish spin 0 from spin $^1/_2$ at the 5σ level [27], provided beamstrahlung effects can be corrected for. As for measuring $m_{\tilde{\mu}}$, Fig. 12b shows that a measurement of the total cross-section at $E_{cm} = 2$ TeV can give an error of 10% on the mass if $m_{\tilde{\mu}} \approx 500$ GeV. Once such a measurement was made, one could reduce the centre-of-mass energy and measure the threshold rise at $E_{cm} \geq 2m_{\tilde{\mu}}$, thereby determining $m_{\tilde{\mu}}$ with an error of 2%, as also seen in Fig. 12b [27].

2.1.4 Comparison of supersymmetry limits

This is complicated by the facts that hadron and lepton accelerators tend to produce different types of sparticles—for example the LHC can produce heavy, strongly interacting sparticles such as gluinos, which do not have electroweak interactions, whereas CLIC can produce all heavy, electroweakly interacting sparticles, including sleptons. In general, it can be concluded from the above studies that CLIC, with an integrated luminosity of about 50 fb^{-1} at $E_{cm} = 2$ TeV, would allow detection of almost all sparticles with electroweak couplings in the mass range of 500 GeV to 850 GeV. In addition, the clean signature of the events would allow one to identify their supersymmetric nature and to measure the detailed properties of the newly found particles. However, since the gluino could be produced only via the decays $\tilde{q} \to q\tilde{g}$, only indirect information could be obtained.

The LHC machine can only produce sparticles with masses O(1) TeV with observable cross-sections if they are strongly interacting, i.e. squarks or gluinos. Because of the high and difficult background situation for jets in such a machine, an analysis to prove the presence of squarks and gluinos is very complicated. However, we think that it is possible to detect or exclude these sparticles up to masses of about 1 TeV. Table 4 summarizes the possible mass limits from different accelerators for each sparticle type. Model-dependent assumptions used in obtaining some of the limits are also shown. We have indicated in italics those bounds which we believe can be established, but which need further evaluation before they can be confirmed.

It is impossible to compare the significance of bounds on different sparticle species in a model-independent way, so we have tried to compare the different rows in Table 4 using two theoretical models [7]. One is the minimal supersymmetric Standard Model (MSSM), which has two bare supersymmetry-breaking mass parameters (m_0, $m_{1/2}$) in terms of which the observable sparticle masses can be estimated as in Eq. (2.11). The other is a minimal superstring-inspired model (MSIM), which has one supersymmetry-breaking mass parameter $m_{1/2}$, and the physical masses are related to it in somewhat different ways [9]:

$$m_{\tilde{q}} \simeq 1.9m_{1/2}\,, \qquad m_{\tilde{g}} \simeq m_{1/2}\,, \qquad m_{\tilde{\gamma}} \simeq 0.16m_{1/2}, \qquad (2.21)$$
$$m_{\tilde{q}_{L,R}} \simeq (0.7, 0.4)m_{1/2}\,, \qquad m_{\tilde{W}} \simeq 0.3m_{1/2}\,.$$

Within these model assumptions, it can be seen that a slepton mass of about 1 TeV corresponds to a squark mass of about 3 to 5 TeV. However, this and the previous model are used only as guides to the relative powers of the different accelerators.

The significance of the present sparticle mass limits (2.1) and (2.2) as bounds on the parameters (m_0, $m_{1/2}$) of the MSSM is shown in Fig. 13a. We see that present-day $p\bar{p}$ and e^+e^- limits are almost equally powerful in constraining the model. Figure 13b shows the corresponding bounds which could be obtained from the new accelerators discussed above, as compiled in Table 4. We see that CLIC at $E_{cm} = 2$ TeV reaches further into the (m_0,$m_{1/2}$) plane than does the LHC at $E_{cm} = 17$ TeV, although this conclusion only holds if CLIC attains the

Table 4

Comparison of possible mass limits from the different accelerators

sparticle type	hh $\sqrt{s}$ = 17 TeV	ep $\sqrt{s}$ = 1.8 TeV	e^+e^- $\sqrt{s}$ = 2 TeV ($\int L\,dt$ = 500 fb^{-1})
slepton	$\tilde{e}, \tilde{\mu}$ 300 GeV	$\tilde{e}$ 350 GeV $m_{\tilde{e}} = m_{\tilde{q}}$	$\tilde{e}, \tilde{\mu}, \tilde{\tau}$ 850 GeV
squark	1 TeV $m_{\tilde{q}} \ll m_{\tilde{g}}$	700 GeV $m_{\tilde{e}}$ = 50 GeV 350 GeV $m_{\tilde{e}} = m_{\tilde{q}}$	850 GeV
wino $^{\pm}$	*450 GeV* $m_{\tilde{W}} = m_{\tilde{q}}$	No useful limit	850 GeV
gluino	*1 TeV* $m_{\tilde{g}} \ll m_{\tilde{q}}$	No useful limit	No useful limit

The limits in *italics* need more study

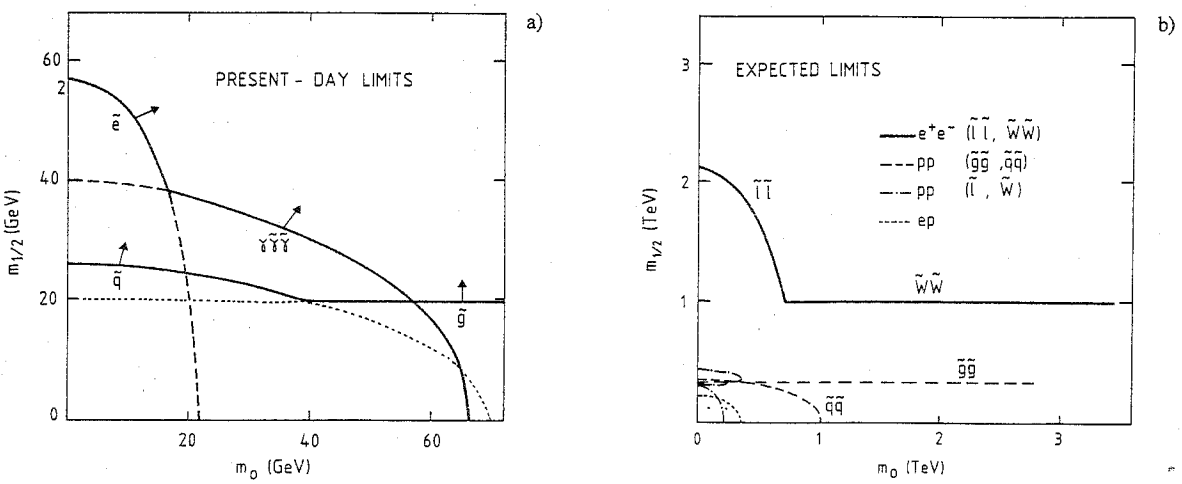

Fig. 13 Significance of sparticle mass limits as bounds on the parameters (m_0, $m_{1/2}$) of the MSSM a) for present sparticle mass limits, and b) for the accelerators discussed in this summary report

luminosity (2.17): otherwise the event rate is not sufficient to discover and study sparticles within one year. In this particular model, as shown in Fig. 13b, the physics reach in the (m_0,$m_{1/2}$) plane of the LHC turns out to be roughly equivalent to that of an e^+e^- collider with E_{cm} = 1 TeV, whilst CLIC has a comparable reach to the SSC with E_{cm} = 40 TeV. Although they are not shown, similar conclusions apply to the comparison in the MSIM.

It should be noted that the overall scales in Fig. 13b are 50 times larger than those in Fig. 13a. Recall also that theory expects, on the basis of the hierarchy argument reviewed in Section 1, that sparticles should weigh $\leq$ 1 TeV [7].

2.2 Z′ physics

Many different possible additional neutral gauge bosons Z′ occur in different models with different couplings. 'Traditional' Z′ bosons such as those appearing in $SU(2)_L \times SU(2)_R \times U(1)$ models have often been considered in previous studies [1, 2], and some composite model Z′-like isoscalar vector bosons are discussed in subsection 2.4. Here we concentrate on novel and speculative Z′ possibilities.

It may be that the TOE is some superstring theory, which may have an underlying $E_8 \times E_8'$ gauge group whose observable part is some subgroup of E_6. This subgroup may be $SU(3)_c \times SU(2)_L \times U(1)_Y \times$ [U(1) or $U(1)^2$], which may break down to the Standard Model $SU(3)_c \times SU(2)_L \times U(1)_Y$ at relatively low energies $\leq$ 1 TeV. If so, there would be one (or two) new Z′ with masses in this range [9]. Clearly this scenario is uncertain and ambiguous, but there are three favoured possibilities for the new Z′ and its couplings [28]. In model A, there is a unique extra U(1) gauge group in four dimensions, whilst in models B and C one starts from a theory with two extra U(1) gauge groups and reduces these down to one at high energies via a large vacuum expectation value (v.e.v.) for either B, an $SU(3)_c \times SU(2)_L \times U(1)_Y$ singlet field N or C, a conjugate sneutrino field $\tilde{\nu}^c$. The extra hypercharge couplings to all the known particles are fixed in each of these models, as shown in Table 5, and the magnitude α' of their gauge coupling strength is fixed by renormalization effects: $\alpha' = 0.015$.

Table 5

Possible neutral currents in superstring models [28]

	T_{3L}	$\sqrt{(5/3)}Y$	$\sqrt{(5/3)}Y'$	Y''
u_L^d	$\pm 1/2$	$1/6$	$1/3$	0
u_L^c	0	$-2/3$	$1/3$	0
d_L^c	0	$1/3$	$-1/6$	$1/2$
$(\nu,\ell)_L$	$\pm 1/2$	$-1/2$	$-1/6$	$1/2$
e_L^c	0	1	$1/3$	0
D_L	0	$-1/3$	$-2/3$	0
D_L^c	0	$1/3$	$-1/6$	$-1/2$
ν_L^c	0	0	$5/6$	$-1/2$
N_L	0	0	$5/6$	$1/2$
$(H^+,H^0)_L$	$\pm 1/2$	$1/2$	$-2/3$	0
$(\bar{H}^+,\bar{H}^0)_L$	$\pm 1/2$	$-1/2$	$-1/6$	$-1/2$

Model A: Z′ couples to Y′
Model B: Z′ couples to $(\sqrt{(3/8)}\,Y' - \sqrt{(5/8)}\,Y'')$
Model C: Z′ couples to $(\sqrt{(3/8)}\,Y' + \sqrt{(5/8)}\,Y'')$

In each model the additional Z′ can mix with the conventional Z, so the model parameters can be characterized as a new mass m′ and a mixing angle Θ. These parameters are determined in any given model by the v.e.v.'s of generalized Higgs fields. In model A, these v.e.v.'s are those of supersymmetric Standard Model Higgses: $v \equiv \langle 0|H|0\rangle$, $\bar{v} \equiv \langle 0|\bar{H}|0\rangle$, and an additional v.e.v., $x \equiv \langle 0|N|0\rangle$. The squared mass matrix in model A is

$$\mathfrak{M}^2 = m_Z^2 \begin{bmatrix} 1 & 1/3\,\sin_w\,[(4v^2 - \bar{v}^2)/(v^2 + \bar{v}^2)] \\ 1/3\,\sin\theta_w\,[(4v^2 - \bar{v}^2)/(v^2 + \bar{v}^2)] & 1/9\,\sin^2\theta_w\,[(25x^2 + 16v^2 + \bar{v}^2)/(v^2 + \bar{v}^2)] \end{bmatrix} \qquad (2.22)$$

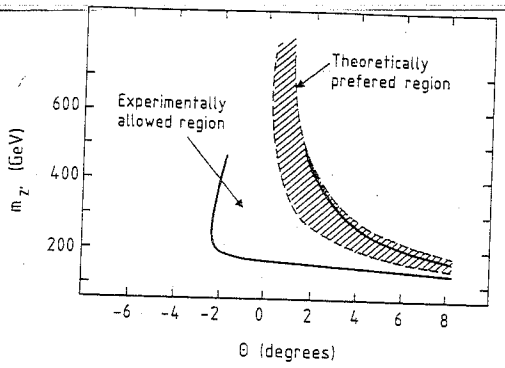

Fig. 14 Constraints [29] on possible values of $(m_{Z'}, \Theta)$ from theory (hatched area) and present experiments (solid lines)

where m_Z is the Standard Model Z^0 mass. Once the Standard Model gauge-boson masses are fixed, this model has two parameters $(x/v, \bar{v}/v)$ which specify the two quantities (m', Θ) introduced earlier. As seen in Fig. 14, the form (2.22) of the mass-squared matrix imposes important constraints on the possible values of (m', Θ).

Significant present-day limits on superstring Z′ bosons come from low-energy neutral-current experiments (deep-inelastic $\nu N \to \nu X$ scattering in particular), from the non-observation of any Z′ at the CERN $p\bar{p}$ Collider, and from the agreement of the observed Z^0 mass with the Standard Model prediction $m_W/\cos\theta_W$. Figure 14 shows the domain of the (m', Θ) plane from Model A which is allowed after combining all these constraints [29]. We see that

$$m_{Z'} \geq (120 \text{ to } 180 \text{ GeV}) \tag{2.23}$$

in the context of the squared-mass matrix (2.22).

Possible future limits on the model parameters will come from searches at the FNAL Tevatron Collider [30], and from precision measurements of neutral-current effects at the Z^0 peak in e^+e^- annihilation [31], with the latter likely to be more stringent. A precision measurement of the forward-backward asymmetry A_{FB} for $e^+e^- \to \mu^+\mu^-$ on the Z^0 peak at LEP could be sensitive to

$$m_{Z'} \approx 500 \text{ GeV}, \tag{2.24}$$

whilst measurements of the left–right polarization asymmetry on the Z^0 peak at the SLC or LEP could be sensitive to

$$m_{Z'} \approx 1.1 \text{ TeV} \tag{2.25}$$

or more [32], depending on details of the model.

2.2.1 Z′ in pp collisions

We have considered the production [28] of the Z′ and its detection [33] via four different decay modes.

1) $Z' \to e^+e^-$: Figure 15a shows the rates for $pp \to (Z' \to e^+e^-) + X$ in the models A, B, and C introduced above. The solid and dash-dotted curves correspond to the cases where the Z′ decays only into Standard Model particles. The other two curves correspond to the cases where the Z′ decays into all particles and sparticles in a 27 of E_6. Models A and C give very similar results for the cross-section calculation. We see that in many cases there is an observable event rate for

$$m_{Z'} \approx (4 \text{ to } 5) \text{ TeV} \tag{2.26}$$

with 10 fb^{-1} at the LHC [28]. No significant background is expected for this decay mode. In order to investigate the influence of the detector, we have implemented the following cuts for electron detection:

$$p_{T1} > 20 \text{ GeV}, \quad p_{T2} > 10 \text{ GeV}, \quad 25° < \Theta < 155°, \tag{2.27}$$

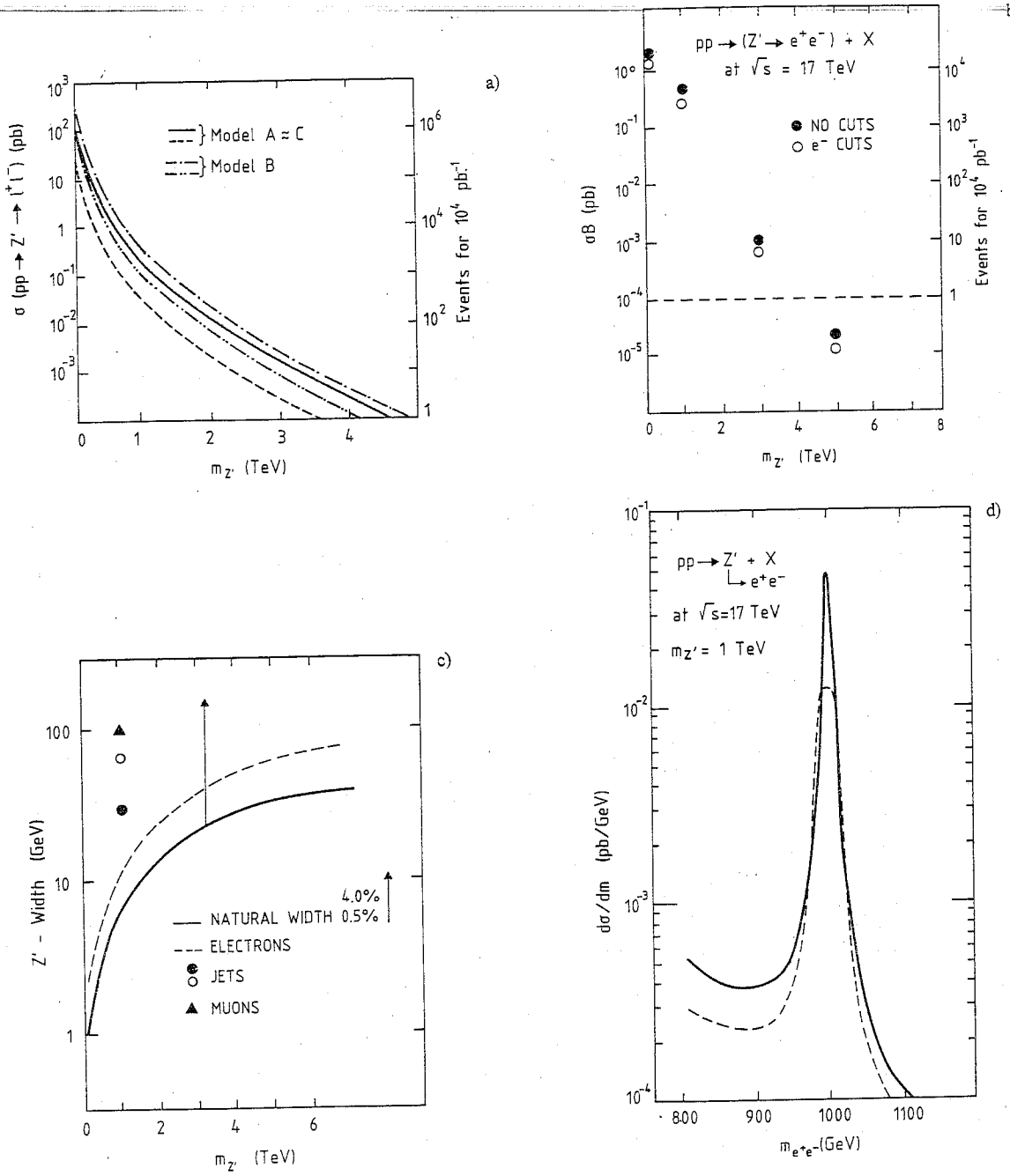

Fig. 15 Cross-sections for $pp \to (Z' \to e^+e^-) + X$: a) for Models A, B, and C (see text); b) Model A with and without electron detection cuts; c) Z' width as a function of $m_{Z'}$ for electrons, muons, and jets using the standard detector resolutions; and d) expected mass distribution for $Z' \to e^+e^-$ before (solid line) and after (dashed line) electron detection cuts (see Ref. [33])

which reduce the observable cross-section by a factor ≈ 2 as seen in Fig. 15b for Model A [33]. We have also incorporated the effects of detector resolution, which gives the apparent Z' widths shown in Fig. 15c. The natural width of the Breit–Wigner $Z' \to e^+e^-$ peak is broadened, but it can probably still be measured if $\Gamma(Z' \to \text{all})/m_{Z'} \geq 0.01$. The effect of the electron detection cuts on there constructed $m_{e^+e^-}$ is compared with the theoretical prediction in Fig. 15d.

2) $Z' \to \mu^+\mu^-$: In this case the rate is the same as for the previous case and the backgrounds are also negligible, but the mass resolution is considerably worse, as seen in Fig. 15c. We expect a mass resolution $\Delta m_{Z'} \approx 100$ GeV

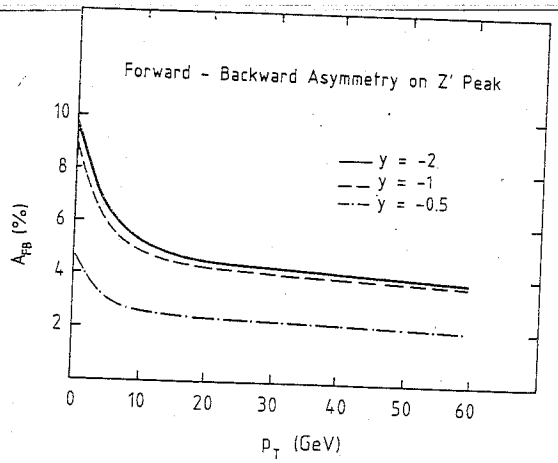

Fig. 16 Forward–backward asymmetry [34] for Model A on the Z′ peak

for $m_{Z'} \approx 1$ TeV. The advantage of this channel is that it can be studied even at higher pp luminosities such as 10^{34} cm^{-2} s^{-1} or more as proposed in some LHC options. This would allow one to explore $m_{Z'} \approx 5$ to 6 TeV [33]. The QCD corrections to the cross-sections for pp $\rightarrow (Z' \rightarrow \ell^+\ell^-) + X$ are also available [34], including p_T distributions and the forward–backward asymmetry. Figure 16 shows the forward–backward asymmetry for Model A in different ranges of p_T and y. The asymmetry vanishes at y = 0 and is unfortunately too small to be measured unless $m_{Z'}$ is quite small, enabling large statistics to be gathered.

3) $Z' \rightarrow q\bar{q}$: This is expected to be the dominant Z′ decay but is subject to a large QCD background, which may make it impossible to see. (We recall that so far there is only a 3σ signal in the UA2 experiment [35] for the W and $Z^0 \rightarrow q\bar{q}$, despite their intrinsically larger couplings to $q\bar{q}$.) As an example of the problems to be faced in a search for $Z' \rightarrow q\bar{q}$, we record the following numbers. For $m_{Z'} = 1$ TeV in Model A, we expect $\sigma B(Z' \rightarrow q\bar{q}) \approx$ 10 pb, corresponding to 5×10^4 events in a detector with efficiency $\epsilon = 0.5$ for an integrated luminosity of 10 fb^{-1}. This is to be compared with the QCD background in three bins of width $\Delta m = 100$ GeV (the resolution taken from Fig. 15c), which we estimate at 6000 pb corresponding to 3×10^7 events (assuming $\epsilon = 0.5$ and $\int L\,dt$ = 10 fb^{-1} as before), with a statistical error of 6×10^3 events. Thus in this case statistics alone would allow an 8σ bump, but to realize this would require very good control of systematic errors and the ability to process $O(10^8)$ complicated events.

4) $Z' \rightarrow W^+W^-$: In many models this has a branching ratio comparable to that for $Z' \rightarrow e^+e^-$, yielding $\sigma B(Z' \rightarrow W^+W^-) \approx 0.5$ pb if $m_{Z'} = 1$ TeV [30]. The best channel for detecting this decay seems to be via ($W_1 \rightarrow$ jet + jet) ($W_2 \rightarrow \ell\nu$), which has $\sigma B_1 B_2 \approx 0.17$ pb corresponding to 800 events in a detector with $\epsilon = 0.5$ and 10 fb^{-1} of luminosity. The W^+W^- continuum background in three bins of $\Delta m = 100$ GeV is 0.05 pb, giving $\sigma B_1 B_2 = 0.017$ pb in the channel ($W_1 \rightarrow$ jet + jet)($W_2 \rightarrow \ell\nu$), but it is estimated that the rate for the QCD background events with indistinguishable topology is about 70 times higher [36], corresponding to a cross-section of 1.2 pb or 6000 ± 80 events in a detector with $\epsilon = 0.5$ and 10 fb^{-1}. Thus it seems that the Z′ may still be detectable in this channel, at least if it has previously been observed in $Z' \rightarrow \ell^+\ell^-$.

In summary, one can search for Z′ with masses up to 4 TeV using the $Z' \rightarrow e^+e^-$ decay channel, and 5 TeV if one uses $Z' \rightarrow \mu^+\mu^-$ running the LHC at $L \approx (10^{34}$ to $10^{35})$ cm^{-2}. If a Z′ with mass ≤ 4 TeV is found, its W^+W^- decay mode can probably also be measured, but looking for $Z' \rightarrow q\bar{q}$ appears very difficult.

2.2.2 Z′ in ep collisions

Here the cross-sections for direct production of the Z′ are too small to be observable, and we must rely on the search for indirect effects detectable by measuring different asymmetries. We assume that $e^{\pm}_{L,R}$ are all available with the same luminosity, which may only be true for e^+ beams of energy ≤ 50 GeV giving $E_{cm} \leq 1.4$ TeV, since

Table 6

Asymmetries measured in ep collisions and their sensitivities [37] to Models A, B, and C

	A	B	C
$e_L^- - e_R^-$	*	*	
$e_L^+ - e_R^+$			*
$e_L^- - e_L^+$			*
$e_R^- - e_R^+$	*		
$e_L^- - e_R^+$			
$e_R^- - e_L^+$	*		*

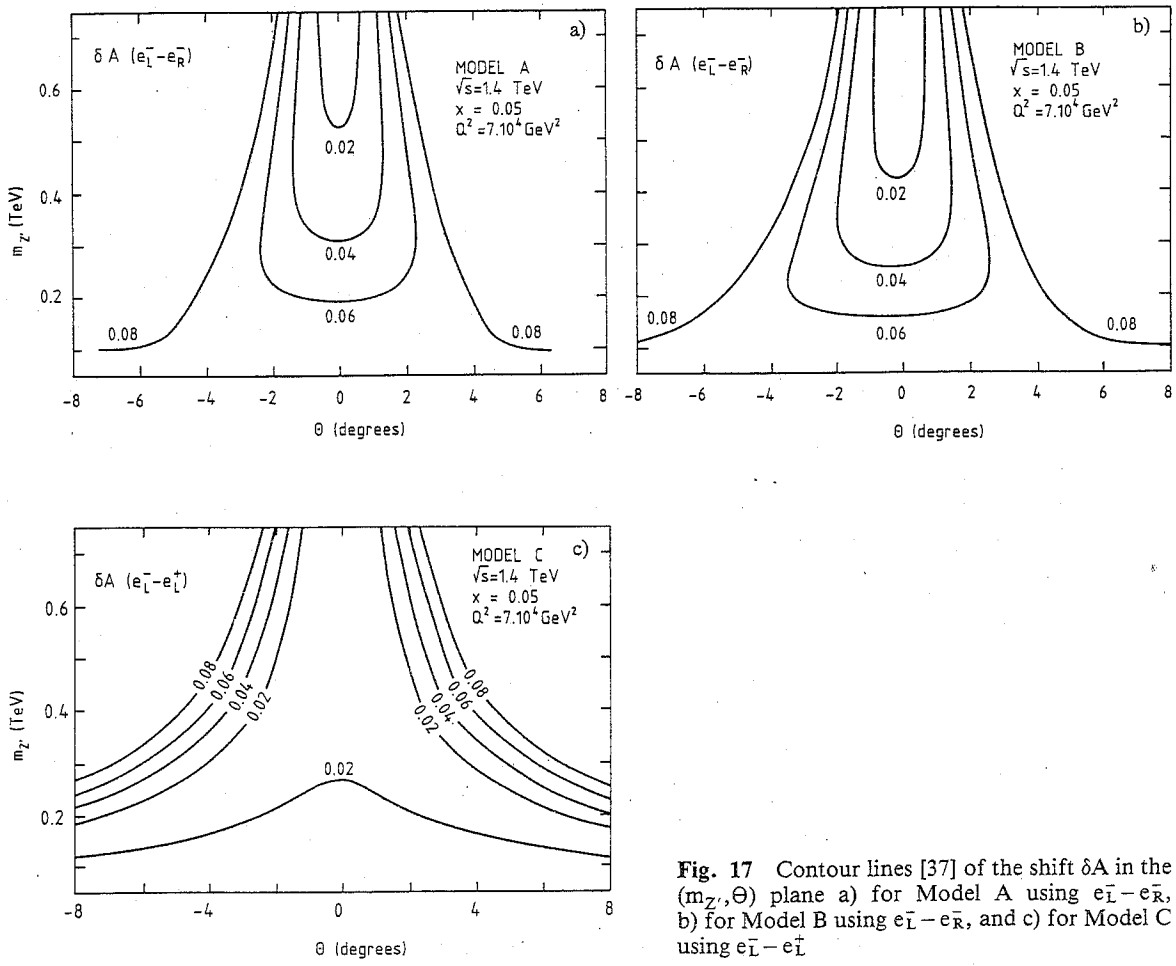

Fig. 17 Contour lines [37] of the shift δA in the $(m_{Z'}, \Theta)$ plane a) for Model A using $e_L^- - e_R^-$, b) for Model B using $e_L^- - e_R^-$, and c) for Model C using $e_L^- - e_L^+$

polarized e^+ beams are unlikely to be available at LEP 200. We can construct six different asymmetries between the four cross-sections with $e^{\mp}_{L,R}$ beams, and we have studied which asymmetries are most sensitive to which models [37]. The conclusions for the Models A, B, and C introduced above are shown in Table 6, under the simplifying assumption that the mixing angle Θ is negligibly small and considering measurements at $E_{cm} = 1.4$ TeV, $x = 0.05$, and $Q^2 = 7 \times 10^4$ GeV^2.

The statistical errors which can be expected in asymmetry measurements are $\delta A = 0.03$ to 0.05, if one uses data in the range $Q^2 = 6.3 \times 10^4$ GeV^2 to 10^5 GeV^2 integrated over x from a run of 1 fb^{-1} with 100% beam polarization. The systematic errors due to uncertainties in the luminosity and in the beam polarization can be removed by measuring simultaneously the same asymmetry at lower Q^2, where it can be compared confidently with the Standard Model prediction. We believe the systematic error can be controlled sufficiently well so that an overall error $\delta A \approx 0.02$ to 0.04 is attainable. Figures 17a to 17c show contours of the shifts δA in favourable asymmetries over the $(m_{Z'},\Theta)$ plane for Models A, B, and C respectively. Comparing Fig. 17a with the region of the $(m_{Z'},\Theta)$ plane which is theoretically favoured by the squared-mass matrix (2.22) for Model A, as seen in Fig. 14, we conclude that these asymmetry measurements give access to [37]

$$m_{Z'} \approx 500 \text{ GeV} . \tag{2.28}$$

This is comparable to the physics reach [Eqs. (2.23) and (2.24)] of asymmetry measurements on the Z^0 peak at LEP [32], and could be useful in distinguishing between possible sources of any discrepancy from the Standard Model which might be seen there.

2.2.3 Z′ in e^+e^- collisions

CLIC could be a Z′ factory—perhaps after the discovery of the Z′ at the LHC—in much the same way as the SLD and LEP follow on after the Z^0 discovery at the CERN $p\bar{p}$ Collider. Treating the Z′ as a conventional Breit-Wigner resonance, the cross-section on the peak is given by unitarity to be:

$$\sigma(e^+e^- \to Z' \to X)/\sigma_{pt} = (9/\alpha^2)B(Z' \to e^+e^-)B(Z' \to X) . \tag{2.29}$$

The e^+e^- branching ratios in the superstring models described earlier vary between 0.6% (Model A, three complete generations of particles and sparticles in **27** representations of E_6) and 6% (Model B, three generations of conventional quarks and leptons only). Putting a typical branching ratio $B(Z' \to e^+e^-) = 1\%$ into (2.29), we get [38] a total cross-section on the Z′ peak of

$$\sigma(e^+e^- \to Z' \to \text{all}) = 0.13/[m(\text{TeV})]^2 \text{ nb} . \tag{2.30}$$

Thus for m = 1 (4) TeV and $L = 10^{33}$ cm^{-2} s^{-1}, one has 1 event per 8 s (1 event per 2 min). However, before we get carried away, we should compare the centre-of-mass energy spread with the natural width of the Z′,

$$\Gamma(Z' \to \text{all})/m_{Z'} = (0.65 \text{ to } 3.8)\% , \tag{2.31}$$

where the minimum is for Models A and B with only decays into conventional quarks and leptons, and the maximum is for a Z′ in any of the models decaying into full **27** representations of particles and sparticles. The natural width (2.31) is smaller than the centre-of-mass energy spread, which is not negligible in linear e^+e^- colliders [11]. Figure 18 shows an example of the centre-of-mass spectrum for a Z′ at $m_{Z'} = 2$ TeV, folded with the machine resolution as compared to a pure Breit-Wigner shape. At the peak the rates drop by more than a factor of 3. We have assumed $B(Z' \to e^+e^-) = 1\%$ and folded in bremsstrahlung (which causes a non-Gaussian energy spread), a beam energy spread of 1% (taken to be Gaussian), and a Breit-Wigner peak with $\Gamma(Z' \to \text{all})/m_{Z'} = 0.02$.

The rates [39] at the Z′ peak for several different CLIC design parameter choices are shown in Table 7. The centre-of-mass energy spread of the machine reduces the rate computed using a naïve Breit-Wigner [Eqs. (2.29) and (2.30)] by a factor of up to 6. Nevertheless, in a typical 'year' of 10^7 s one should hope to accumulate between

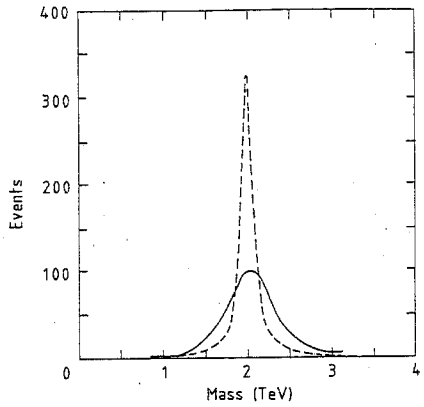

Fig. 18 Centre-of-mass spectrum of a Breit–Wigner resonance at $m_{Z'} = 2$ TeV for CLIC with a disruption parameter of 1.7 folded with a Gaussian beam spread of 1% (full curve). For comparison a pure Breit–Wigner shape is shown (dashed curve).

Table 7

Expected rates [38, 39] at the Z′ peak [$\Gamma(Z' \to \text{all})/m_{Z'} = 0.02$] for different CLIC design parameter choices in 10^7 s (= 'year')

c.m.s. energy (TeV):	1		2		
Disruption:	0.56	3.0	0.32	0.70	1.5
Luminosity ($cm^{-2}\,s^{-1}$):	6×10^{31}	10^{33}	6×10^{31}	2×10^{32}	10^{33}
Number of events with					
1) no beam radiation + no beam spread	7.2×10^4	1.2×10^6	2.0×10^4	6.0×10^4	3.0×10^5
2) beam radiation + 1% Gaussian spread	2.2×10^4	3.5×10^5	6.0×10^3	1.8×10^4	8.8×10^4

2×10^4 and 2×10^5 Z′ decays. Notice that parameter choices with larger disruption D and hence larger bremsstrahlung effects nevertheless give larger event rates on the Z′ peak, because their higher luminosities overcome the increase in the centre-of-mass energy spread [39].

With a sample of 10^4 to 10^5 Z′ events, one can consider searching for rare Z′ decays. The following candidates come to mind:

i) $Z' \to W^+W^-$: This is not really a rare decay mode, since its decay branching ratio, whilst model-dependent, is typically of the same order as $B(Z' \to e^+e^-) \approx (1 \text{ to } 3)\%$ [30].

ii) $Z' \to d\bar{D}_{1/2} + \bar{d}D_{1/2}$: This is a flavour-changing Z′ decay, with d a generic, light charge, $-1/3$ quark (d, s, or b), and $D_{1/2}$ a heavy charge, $-1/3$ colour-triplet fermion with a leptoquark or diquark decay signature (see subsection 2.3): $D_{1/2} \to \ell q\tilde{\gamma}$ or $\bar{q}\bar{q}\tilde{\gamma}$. The branching ratio for this decay would be of order

$$\frac{\Gamma(Z' \to d\bar{D}_{1/2} + \bar{d}D_{1/2})}{\Gamma(Z' \to d\bar{d})} = \min\left[\left(\frac{\langle 0|\tilde{\nu}^c|0\rangle}{\langle 0|N|0\rangle}\right)^2, \quad \left(\frac{\langle 0|N|0\rangle}{\langle 0|\tilde{\nu}^c|0\rangle}\right)^2\right]. \tag{2.32}$$

We do not know what this ratio of v.e.v.'s might be, and a search for (or observation of) this rare Z′ decay would give us valuable information about it.

iii) $Z' \to H'\ell^+\ell^-$: This is the analogue of conventional $Z^0 \to H\ell^+\ell^-$ decay and the relative rate

$$\frac{\Gamma(Z' \to H'\ell^+\ell^-)}{\Gamma(Z' \to \ell^+\ell^-)} \approx O(\sin^4\theta_w)\frac{\Gamma(Z^0 \to H\ell^+\ell^-)}{\Gamma(Z^0 \to \ell^+\ell^-)} \qquad (2.33)$$

for similar values of m_H/m_Z. Formula (2.33) assumes that the $\ell^+\ell^-$ pair emanates from a virtual Z', and gives very small rates unless $m_{H'} \ll m_Z$. However, in some models the decay $Z' \to H' + (Z^0 \to \ell^+\ell^-)$ is also possible, and could have a much larger branching ratio [40].

What if the Z' has not previously been detected at the LHC, and one must scan [41] for it at CLIC? Let us take as an example $m_{Z'} \approx 1$ TeV and assume a luminosity of 10^{33} cm^{-2} s^{-1} at D = 3.0 as in the second column of Table 7. Then the event rate on the Z' peak would be 0.035 s^{-1}. If one goes off resonance by $\Delta E_{cm} = 50$ GeV, the total cross-section is reduced by a factor of ≈ 3, giving an event rate of 0.012 s^{-1}. This is to be compared with a background annihilation rate from R $\approx$ 20 of 0.0018 s^{-1}. A run of 10 hours will therefore give a signal of $\approx$ 180 events above a background of $\approx$ 60 events. Proceeding by two steps per day, one can scan a range of 0.5 TeV in E_{cm} within a week. Scanning for a Z' should therefore be easy [41].

What are the prospects of searching for indirect effects [42] of a heavy Z' which weighs more than E_{cm}? The most sensitive place to look is probably via effects on $e^+e^- \to \mu^+\mu^-$. The angular distribution for this reaction carries essentially the same information as the total cross-section. Assuming L = 4 × 10^{33} cm^{-2} s^{-1} at E_{cm} = 2 TeV, which yields 870 $\mu^+\mu^-$ pairs per year, we expect a statistical error $\delta\sigma/\sigma \approx 3\%$. We believe it is reasonable to expect the absolute luminosity at CLIC to be known to within a few percent, so that the total error $\delta\sigma/\sigma \approx 4\%$ to 10%. Figure 19 exhibits the (x/v, $\bar{v}$/v) parameter space of the MSIM Model A introduced earlier, showing contours of $m_{Z'}$ between 2 and 4 TeV. Also shown are the contours of $\delta\sigma/\sigma$ for $e^+e^- \to \mu^+\mu^-$ of 4%, 6%, and 10%. We see that these can explore indirect Z' effects for $m_{Z'} \leq 3$ to 4 TeV [42]. However, we would not claim these as possible discovery limits for the Z' in e^+e^- collisions, since a small discrepancy from the Standard Model prediction for $\sigma(e^+e^- \to \mu^+\mu^-)$ would be ambiguous, with other possible interpretations (see e.g. sub-subsection 2.4.3).

We close this sub-subsection with a few comments on the problem of luminosity measurement at CLIC. The latest design of the e^+e^- interaction point presented at this meeting has free space in the angular range $10° < \Theta < 170°$, and the possibility of ± 30 cm free space at angles between (2 and 10)° and (170 and 178)°. If the latter are

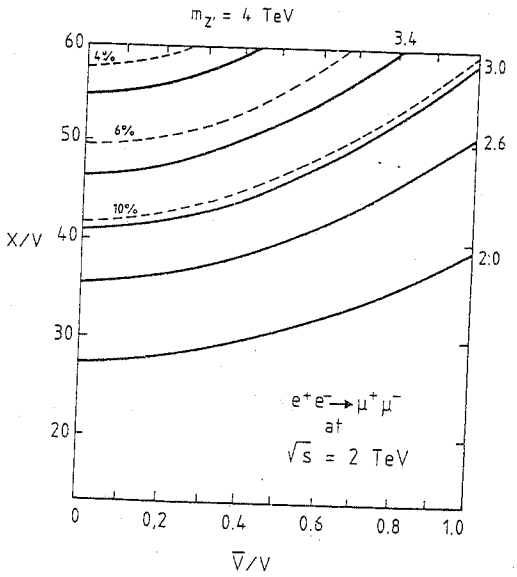

Fig. 19 Contours [42] for $m_{Z'}$ and $\delta\sigma/\sigma$ for $e^+e^- \to \mu^+\mu^-$ in the (x/v, $\bar{v}$/v) plane using the MSIM Model A

indeed available, we see no reason why the luminosity could not be measured as accurately as at PETRA and PEP, i.e. with an error of 4%, using Bhabha events. However, it still seems possible that beamstrahlung-induced γ backgrounds may exclude detectors from the regions $\Theta < 10°$ and $> 170°$, and the existence of a Z′ with unknown mass and width could obscure the interpretation of Bhabha cross-section measurements. Nevertheless, we see a possible way [43] of measuring the luminosity with an error of $\approx 10\%$, based on the following steps, assuming that the Bhabha cross-section can be measured down to $\Theta = 10°$, which yields ≈ 100 events per day. First, assume approximate values for $m_{Z'}$ and $\Gamma_{Z'}$ and incorporate them in a calculation of the cross-section for small-angle Bhabha events. Then, use this cross-section and the observed small-angle event rate to compute a first approximation L_1 to the luminosity. The final step is to check with the event rate of large-angle Bhabha events, comparing the observed number and the expected number, assuming the first approximation L_1 to the luminosity. This enables a second approximation to be computed:

$$L_2 = L_1 \times \sigma(\text{large angle})_{\text{obs, assuming } L_1} / \sigma(\text{large angle})_{\text{expected}} . \tag{2.34}$$

We can now go back to recompute the parameters $(m_{Z'}, \Gamma_{Z'})$ of the possible resonance using as input L_2 and the observed small-angle Bhabha rate. By iteration we can eventually arrive at accurate estimates of $m_{Z'}$, $\Gamma_{Z'}$, and L. As an alternative, it has also been suggested [21] that one might monitor L using a large cross-section $\gamma\gamma$ process such as $e^+e^- \to e^+e^-\mu^+\mu^-$, making cuts $p_T^{\mu} \geq 10$ GeV, which leave a very large event rate. However, here there is the possible theoretical problem of computing the cross-section with a very small error.

2.3 Leptoquarks

Particles with leptoquark quantum numbers appear in many different theoretical frameworks. They could have spin J = 0 or 1, and electric charge Q = $-4/3$, $-1/3$, 2/3, or 5/3. The most common possibility, which we choose to study, is J = 0 and Q = $-1/3$. The couplings of J = 0 leptoquarks are often correlated with fermion masses, and they may well be associated with Higgs boson couplings,

$$g_{LQf\bar{f}} \propto g_{Hf\bar{f}} \propto m_f . \tag{2.35}$$

However, this property is not inevitable. Many approaches [9] to the compactification of the superstring predict that light particles fill out **27** representations of E_6, which contain J = 0, Q = $-1/3$ particles that may have leptoquark couplings whose magnitudes are completely decoupled from those of the Higgs fields. Indeed, the J = 0 particles D_0 which are candidates for leptoquarks could even have diquark couplings instead: $D_0 \to \bar{q}\bar{q}$. Thus the possible generic signatures for the D_0 are given by the following tree:

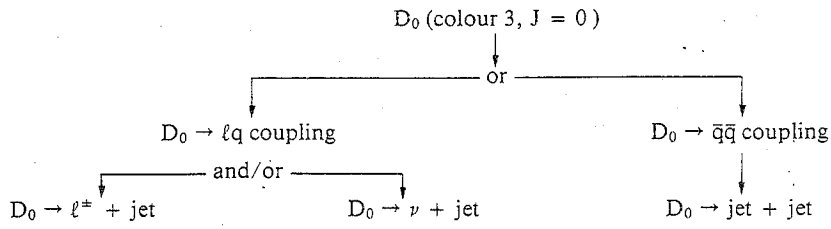

(2.36)

To accompany J = 0 leptoquarks, any supersymmetric theory would predict J = 1/2 supersymmetric partners. In the case of the superstring-inspired model introduced above, where we call these spartners $D_{1/2}$, they could have

$$(D_{1/2} \to \ell^{\pm} + q + \tilde{\gamma} \quad \text{and/or} \quad \nu + q + \tilde{\gamma}) \text{ or } (D_{1/2} \to \bar{q} + \bar{q} + \tilde{\gamma}) \tag{2.37}$$

as generic decay modes. The possible decay chains (2.36) and (2.37) give experimentalists plenty of signatures to explore, namely ($\ell^{\pm}$ + jet) or (jet + jet) mass bumps from D_0 decay, missing-energy events from $D_0 \to \nu$ + jet, $D_{1/2} \to \tilde{\gamma} + \nu$ + jet or $D_{1/2} \to$ jet + jet + $\tilde{\gamma}$, and $\ell^{\pm}$ + jet + missing energy from $D_{1/2}$ decay [44]. In the rest of this subsection we will mainly emphasize the leptoquark decays $D_0 \to \ell^{\pm} + q$, $D_{1/2} \to \ell^{\pm} + q + \tilde{\gamma}$, but the other signatures will also receive some consideration.

Composite models can also yield leptoquark bosons. Of particular interest is the rich spectrum of $J = 0, 1$ leptoquarks with $Q = -1/3, 2/3$ expected in the strongly coupled version of the Standard Model. These leptoquarks are distinguished by the following features: i) any possible conflict with bounds on flavour-changing neutral currents is naturally avoided, and ii) each leptoquark has only two decay channels, $q\ell^{\pm}$ and $q\overset{(-)}{\nu}$, with branching ratios of 50% each. This leads to clear-cut experimental signatures.

2.3.1 Leptoquarks in pp collisions

We have mainly considered the pair-production mechanisms $gg, q\bar{q} \rightarrow D_0\bar{D}_0, D_{1/2}\bar{D}_{1/2}$. As can be seen in Fig. 20, observable rates exist out to masses [45]

$$m_{D_0}, m_{D_{1/2}} \approx 2 \text{ TeV} . \tag{2.38}$$

It should be noted, moreover, that these rates are independent of the unknown magnitude of the $D \rightarrow \ell q$ or $\bar{q}\bar{q}$ coupling. If there was a $D \rightarrow \bar{q}\bar{q}$ coupling, it would enable the D_0 to be produced also singly via $\bar{q}\bar{q}$ annihilation. The rate for this production mechanism depends on the unknown $D \rightarrow \bar{q}\bar{q}$ coupling strength, but it is easily estimated that any $D_0 \rightarrow$ jet + jet mass bump is drowned in QCD background for any plausible magnitude of this coupling strength. Accordingly we concentrate on the observability of the signatures for $D_0\bar{D}_0$ and $D_{1/2}\bar{D}_{1/2}$ pair-production.

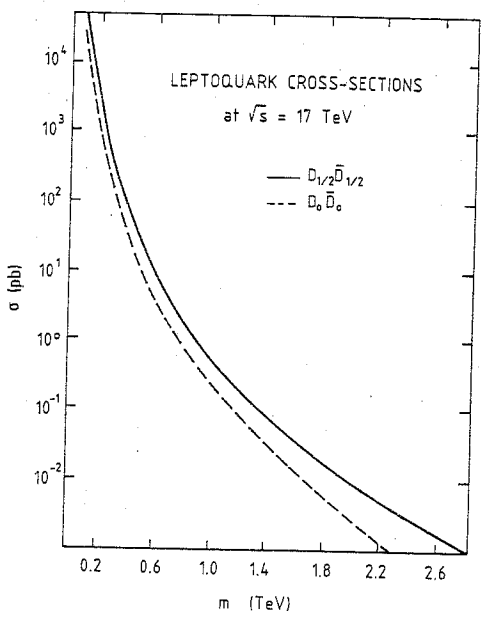

Fig. 20 Leptoquark production cross-sections [45] in a hadron collider at $\sqrt{s} = 17$ TeV

The decays $D_0 \rightarrow q + \nu$ would give signatures very similar to the $\tilde{q} \rightarrow q + \tilde{\gamma}$ decays discussed in sub-subsection 2.1.1. We conclude that in this case there would be sensitivity to D_0 particles with masses up to [16]

$$m_{D_0} \approx 1 \text{ TeV} . \tag{2.39}$$

The pair of $D_0 \rightarrow q + \ell$ decays would give ($\ell^+ + \ell^-$ + jet + jet) final states. The dominant backgrounds are expected to come from pair-production of heavy quarks followed by their semileptonic decays. We have looked in detail at the background from $t\bar{t}$ production decay, and find that simple cuts render it negligible for all values of m_{D_0} and $m_{D_{1/2}}$ if $m_t \leq 110$ GeV. If $m_t \geq 110$ GeV or if there is some other heavier quark Q, the same simple cuts leave $m_{D_{1/2}} \leq 1.2$ TeV. More work is required to beat down the background if m_t (or m_Q) ≥ 110 GeV and m_{D_0}, $m_{D_{1/2}} \geq 1.2$ TeV, but we believe this can easily be done. Therefore the event-rate limit (2.38) is the discovery limit for $D_0 \rightarrow q + \ell$ decays [45]. By contrast, pairs of $D_0 \rightarrow \bar{q}\bar{q}$ decays also seem always to be lost in the background from QCD four-jet events.

One can also look for leptoquarks indirectly in pp collisions, through their possible effects on the Drell-Yan $\ell^+\ell^-$ pair-production cross-section [46], analogous to the composite model contact terms discussed in subsubsection 2.4.1. We find that a 50% measurement of $\sigma(pp \to \ell^+\ell^- + X)$ for $m_{\ell^+\ell^-} \leq 1$ TeV could give sensitivity to [46]

$$m_{D_0} \approx 1.2 \text{ TeV} \sqrt{F}\,, \tag{2.40}$$

where F measures the leptoquark coupling strength

$$g^2_{LQ}/4\pi = F \times \alpha_{em}\,. \tag{2.41}$$

This limit is unlikely to be competitive with the direct limit (2.38), and has the relative disadvantages of being more model-dependent as well as less direct.

2.3.2 Leptoquarks in ep collisions

Here there are simple production mechanisms: $e^- + q \to D_0$ or $e^+ + \bar{q} \to \bar{D}_0$ which could give copious single leptoquark production. The rate clearly depends on $F = g^2_{LQ}/4\pi\alpha_{em}$, but is large enough to be observable for $m_{D_0} \leq 1.6$ TeV at $E_{cm} = 1.8$ TeV if $F = 1$ [47, 48]. If the D_0 has the leptoquark coupling necessary for this production mechanism to exist, it cannot simultaneously have a diquark coupling, and its possible signatures are therefore $D_0 \to q\ell^-$ and/or $D_0 \to q\nu$.

There are no significant backgrounds to searches for $D_0 \to q\mu^-$ or $D_0 \to q\tau^-$, but these decay modes may be suppressed in view of the fact that production occurs via a $D_0 \to qe^-$ coupling. There is a large background to $D_0 \to qe^-$ decays from the continuum of neutral-current events. Nevertheless, a D_0 peak may be visible in the (ℓ + jet) final-state invariant mass, even before cuts, as seen in the upper part of Fig. 21 [48]. The different kinematics of D_0 decay (isotropic and hence flat in y) and of neutral-current events (mainly at low Q^2 and hence at small y) can be exploited to improve the signal-to-background ratio, as shown in the lower part of Fig. 21. The rates for signal and backgrounds with $y > 0.5$ are shown as functions of m_{D_0} in Fig. 22. The dominant background to a search for $D_0 \to q + \nu$ decay comes from conventional charged-current events $ep \to \nu + X$. As seen in Figs. 21 and 22, a y-cut

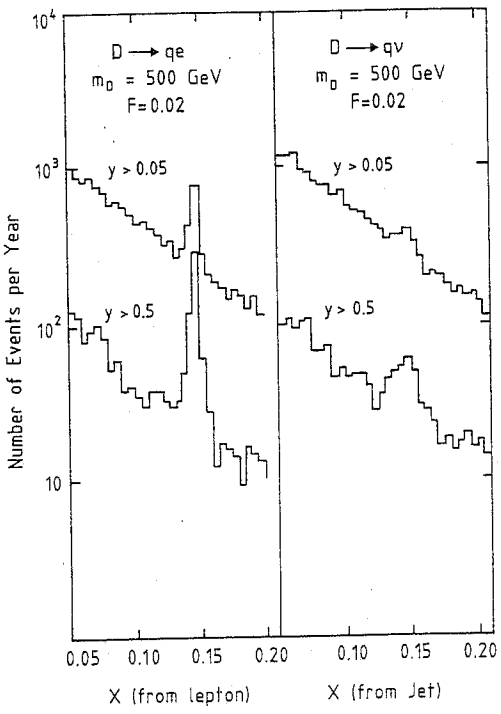

Fig. 21 Number of expected events per year for leptoquark decays in ep collisions [47, 48], assuming $m_{D_0} = 500$ GeV and $F = 0.02$

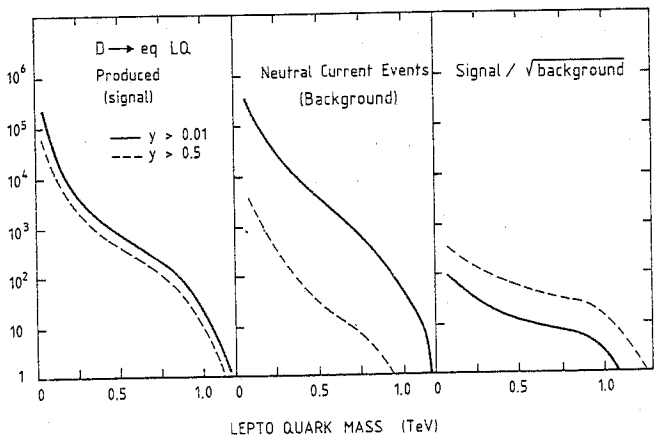

Fig. 22 Expected rates [48] for leptoquarks and for background neutral-current events as a function of m_{D_0} in ep collisions

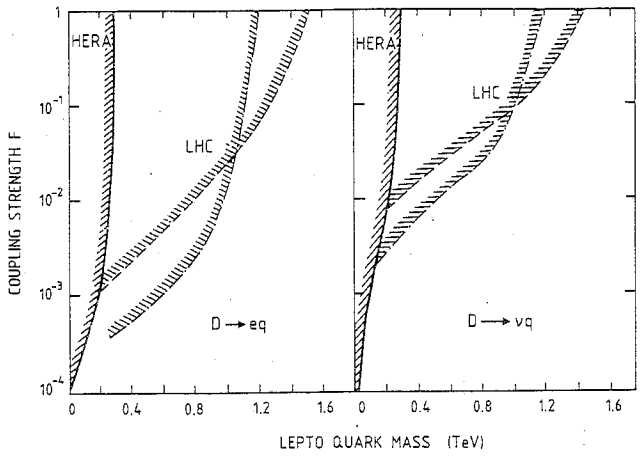

Fig. 23 Observability [48] of the D_0 in ep collisions at HERA and LHC

similar to that used for reducing the neutral-current background can also be used to reduce the charged-current background and thereby render $D_0 \to q + \bar{\nu}$ decay observable [48].

Figure 23 summarizes our conclusions on the observability of the D_0 in ep collisions at HERA as well as at the LHC. We see that for $F = 1$ one can reach almost to the kinematic limit

$$m_{D_0} \approx 1.6 \text{ TeV} \tag{2.42}$$

at $E_{cm} = 1.8$ TeV [48]. This is one case where the higher-energy LHC ep option has a clear advantage.

We have also studied the indirect effects of virtual D_0 exchange on the neutral-current cross-section for $ep \to e + X$, as a way to probe for $m_{D_0} \geq E_{cm}$. However, we find that such effects are negligible for $D_0 \geq E_{cm}$ if $F \leq 1$ [47].

2.3.3 Leptoquarks in e^+e^- collisions

Unless there are large Yukawa couplings, the dominant production mechanisms are $e^+e^- \to (\gamma,Z,Z')^* \to D_0\bar{D}_0$, $D_{1/2}\bar{D}_{1/2}$. Because the D_0 has spin 0 and $Q_{em} = -1/3$, the rate for $e^+e^- \to \gamma^* \to D_0\bar{D}_0$ is very small,

$$R \equiv \sigma(e^+e^- \to \gamma^* \to D_0\bar{D}_0)/\sigma_{pt} = (1/12)\beta^3 , \qquad \beta = \sqrt{(1-4m_{D_0}^2/s)} , \tag{2.43}$$

and this is not greatly improved by including the Z^* and Z'^* exchanges. On the other hand, the rate for $e^+e^- \to \gamma^* \to D_{1/2}\bar{D}_{1/2}$ is significantly larger, with $R \to 1/3$ at large $E_{cm} \gg m_{D_{1/2}}$, and a threshold rise $\propto \beta$. Figures 24a and 24b show the rates for $D_0\bar{D}_0$ and $D_{1/2}\bar{D}_{1/2}$ pair-production in two different cases: a) with no Z' contribution, and b) on the Z' peak, which is assumed to be at the E_{cm} of the corresponding CLIC option [49]. In view of the small event rates in Fig. 24a, we consider that

$$L = 10^{33} (E_{cm}/1 \text{ TeV})^2 \text{ cm}^{-2} \text{ s}^{-1} \tag{2.44}$$

is necessary to be able to do D_0 physics in e^+e^- collisions.

Among the backgrounds considered are: i) $e^+e^- \to q\bar{q}$; ii) $e^+e^- \to Q\bar{Q}$ or $L\bar{L}$ from a fourth generation; iii) $e^+e^- \to W^+W^-$ and Z^0Z^0; and iv) two-photon processes. To simulate these and the signal process, we have used the Lund e^+e^- event generator including initial-state radiation, electroweak corrections to γ^*exchange, and second-order QCD for the hadronic final states. As discussed in detail in a contribution [49] to this study, it was found that any D_0 or $D_{1/2}$ final state could be picked out with high efficiency by cuts that suppressed the background below the level of the signal. As an example, we quote the case of the $D_0 \to ue^-$ decay mode. A

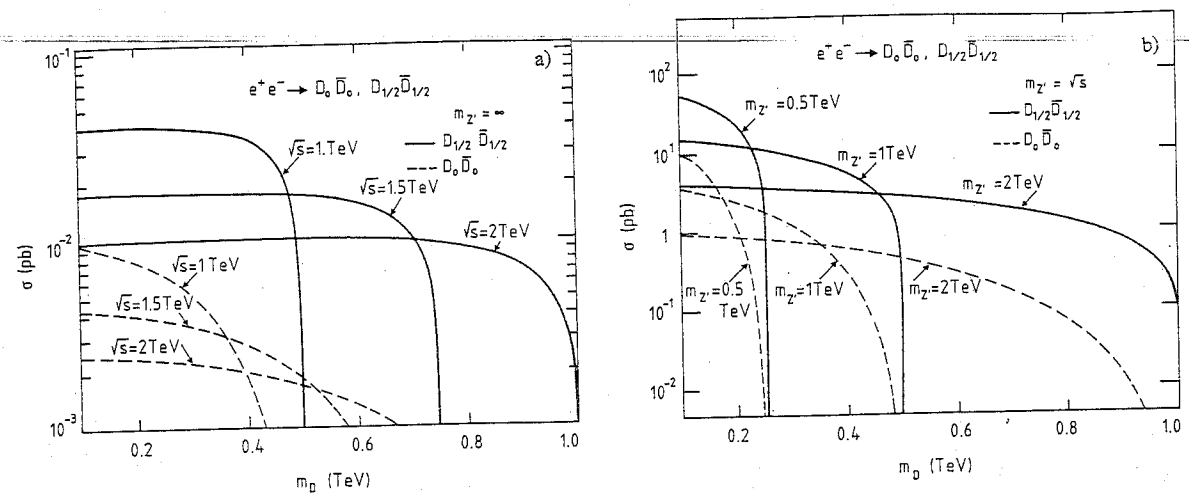

Fig. 24 Leptoquark pair-production [49] in e^+e^- collisions: a) with no Z′ contribution and b) on the Z′ peak which is assumed to be at the indicated E_{cm} of CLIC

selection of events with an $e^{\pm}$ pair (p_{e_1}, p_{e_2} > 10 GeV), at least two hadronic jets, and m_{D_0} − 40 GeV < m_{ej_1}, m_{ej_2} < m_{D_0} + 60 GeV, had a combined efficiency of 76% and reduced the background by a factor of 10^3 or more. Similar results [49] were found for other D_0 decay modes.

We conclude that the D_0 and $D_{1/2}$ could be detected if they were produced, but that the high luminosity (2.44) would be necessary in the case of the D_0 search in the e^+e^- continuum with no Z′ contribution. In these conditions, the discovery limits would be [49]

$$m_{D_0} \approx 650\ \text{GeV}, \qquad m_{D_{1/2}} \approx 950\ \text{GeV}. \tag{2.45}$$

If there were a Z′ in the CLIC energy range, it would be possible to detect m_{D_0}, $m_{D_{1/2}} \leq 1/2 m_{Z'}$.

We have also considered an indirect search for D_0 exchange which could give a contact term analogous to the terms discussed in the context of composite models in sub-subsection 2.4.3. We find that under assumptions similar to those used in 2.3.3 for the attainable statistical and systematic errors, the following limit could be reached:

$$m_{D_0} \approx 1.8\ \text{TeV} \tag{2.46}$$

at E_{cm} = 2 TeV if F = 1 [49]. However, we do not quote this as a discovery limit in view of its model-dependence and indirect nature.

The leptoquarks of the strongly coupled Standard Model, with J = 0, 1 and Q = −1/3, 1/3, may also be pair-produced in e^+e^- collisions. The J = 0, Q = $-1/3$ leptoquarks manifest themselves in the same way as the D_0 discussed above. The J = 1 leptoquarks do not suffer from the β^3 threshold suppression factor. Therefore they can be detected for all masses essentially up to the beam limit of 1 TeV. An indirect search can also be made, looking for leptoquark exchange contributions to $e^+e^- \to q\bar{q}$, which is sensitive to masses of ≈ 10 TeV if the effective coupling is 1.

2.4 Compositeness

As was mentioned in Section 1, many theorists propose as a solution to the Flavour Problem the possibility that quarks and leptons are composite, whilst others hope to understand the W and Z^0 masses by interpreting them as composite [4]. We denote by Λ the energy scale at which this compositeness would be manifest. The radius R_c of composite states would be related to the corresponding Compton wavelength: $R_c = O(1/\Lambda)$. Among the possible manifestations of compositeness could be contact terms scaled by inverse powers of Λ, form factors $F(Q^2/\Lambda^2)$, and excited states e^*, q^*, V^*, ... with masses O(Λ). There is a common expectation that Λ ≈ (1 to 10) TeV, but this

should be interpreted with caution, since no satisfactory and theoretically consistent composite model yet exists. In what follows, we concentrate on contact interactions and on excited states as possible signatures of compositeness.

We discuss four-fermion contact interactions, using an effective Lagrangian in the notation of Eichten, Lane and Peskin [50]

$$\mathcal{L}_{\text{eff}} = g^2_{\text{eff}} \left[(\eta_{LL}/2\Lambda^2_{LL})(\bar{\psi}_L\gamma^\mu\psi_L)(\bar{\psi}_L\gamma_\mu\psi_L) + (\eta_{RR}/2\Lambda^2_{RR})(\bar{\psi}_R\gamma^\mu\psi_R)(\bar{\psi}_R\gamma_\mu\psi_R) \right.$$
$$\left. + (\eta_{LR}/2\Lambda^2_{LR})(\bar{\psi}_L\gamma^\mu\psi_L)(\bar{\psi}_R\gamma_\mu\psi_R) + (\eta_{RL}/2\Lambda^2_{RL})(\bar{\psi}_R\gamma^\mu\psi_R)(\bar{\psi}_L\gamma_\mu\psi_L) \right], \quad (2.47)$$

where the η_{ij} may be ± 1, and seek to bound the parameters Λ_{ij} using the interferences between $\mathcal{L}_{\text{eff}}$ (2.47) and the conventional gauge interactions. Following convention, we do this assuming $g^2_{\text{eff}} = 4\pi$ in (2.47). When considering the single production of excited quarks or leptons, we use the transition couplings

$$\mathcal{L}_{\text{eff}} = (g/2\Lambda^*)\bar{f}^*\sigma_{\mu\nu}(v - a\gamma_5)fF^{\mu\nu}, \quad (2.48)$$

where $F^{\mu\nu}$ is some gauge field strength, g is the corresponding gauge coupling [e in the case of $U(1)_{em}$, g_2 in the case of $SU(2)_L$, etc.], and $v^2 + a^2 = 1/2$. Rather than explore the full plane of (m_{f^*},Λ^*) values, we will usually quote discovery limits for $m_{f^*} = \Lambda^*$. Note that, because of the way we define Λ in (2.47) and Λ^* in (2.48), we expect $\Lambda^* \approx \sqrt{\alpha,\alpha_2,\alpha_3}\Lambda$.

2.4.1 Compositeness in pp collisions

The possibility of a four-quark contact interaction can best be explored by a detailed study [51] of pp → jet + jet + X. The QCD 2 → 2 subprocesses have characteristic angular distributions which are sharply peaked forward and backward, whilst the conjectured contact terms (2.47) would give more isotropic distributions. Thus a study of the angular distribution of two-jet events is more sensitive than a measurement of the total two-jet cross-section, and is also largely independent of theoretical errors induced by uncertainties in the initial parton distributions and higher-order QCD effects. We use the variable [52]

$$\chi \equiv (1 - |\cos\Theta|)/(1 + |\cos\Theta|) \quad (2.49)$$

to plot the two-jet angular distributions in Fig. 25. Shown there are the expected distributions of jet–jet pairs with masses between 7 and 8 TeV, including a vector–vector (VV) contact term with different values of the compositeness scale $\Lambda_{qq} \equiv \Lambda_{LL} = \Lambda_{LR} = \Lambda_{RL} = \Lambda_{RR}$: Λ_{qq} = 11 TeV, 12 TeV, and ∞ corresponding to pure QCD.

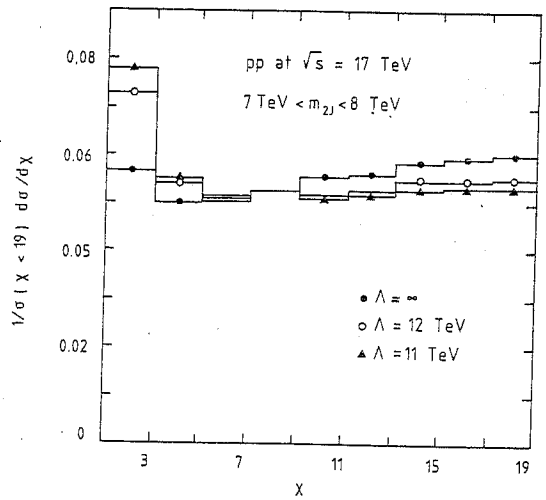

Fig. 25 Expected angular distribution of jet pairs [51] for different Λ values and pure QCD (Λ = ∞) for pp collisions at $\sqrt{s}$ = 17 TeV

The range of jet–jet masses considered is the result of a competition between high sensitivity (large m_{2J}) and large statistics (small m_{2J}): the range shown is not necessarily optimized, but was based on previous experience with UA1 data. The 95% confidence level limit obtainable at the LHC with 10 fb^{-1} was found to be [51]

$$\Lambda_{qq} \approx 12 \text{ TeV}, \tag{2.50}$$

to be compared with $\Lambda_{qq} \geq 415$ GeV from present UA1 data [52].

One can also use pp collider data to probe an eq contact term via the Drell–Yan process $pp \rightarrow e^+e^- + X$. We have not made a detailed estimate of the sensitivity that can be reached with this reaction, but a 50% measurement of $d\sigma/dm_{\ell^+\ell^-}$ for $m_{\ell^+\ell^-} \leq 1$ TeV would be sensitive to

$$\Lambda_{eq} \approx 20 \text{ TeV}, \tag{2.51}$$

where we have again assumed a VV form of interaction with $\Lambda_{eq} \equiv \Lambda_{LL} = \Lambda_{LR} = \Lambda_{RL} = \Lambda_{RR}$ [53].

The final probe of compositeness in pp collisions that we consider is q^* production via $g + q \rightarrow q^*$ and/or $q + q \rightarrow q + q^*$ via contact interactions. The generic form (2.48) of interaction, with $g = g_3$, $F^{\mu\nu}$ the gluon field strength, and $\Lambda^* = m_{q^*}$, can be used to estimate the q^* production cross-section via the first subprocess. One can look for $q^* \rightarrow q + g$ decay through the same interaction as a jet–jet bump on top of the QCD continuum. A theoretical estimate [54] indicates that the signal-to-background ratio falls as m_{q^*} increases, becoming one-to-one when

$$m_{q^*} \approx 5 \text{ TeV}, \tag{2.52}$$

which we take to be the theoretical discovery limit for this type of composite model effect.

2.4.2 Compositeness in ep collisions

Here the principal sensitivity is to an eq contact term. As in the case of different Z′ models, different asymmetries probe contact terms with different combinations of helicities. A complete survey has been made [55] of the relative sensitivities of different asymmetries at $x = 0.05$ and $Q^2 = 7 \times 10^4$ GeV in an ep collider with $E_{cm} = 1.4$ TeV. (The $E_{cm} = 1.8$ TeV ep option would be less sensitive, because of its smaller luminosity.) Four representative asymmetries are shown in Figs. 26a to 26d as functions of Q^2. The effects of the different helicity structures are shown for contact terms with $\Lambda_{eq} = 5$ TeV and positive signs $\eta = +1$ at $\sqrt{s} = 1.4$ TeV and $x = 0.05$. Also shown are the Standard Model predictions for the four asymmetries. Table 8 shows the most sensitive asymmetry for each helicity combination, and the value of Λ_{eq} to which the asymmetry is sensitive with 10^{39} $cm^{-2} = 1$ fb^{-1} of integrated luminosity, after integrating over x. The values lie in the range [55]

$$\Lambda_{eq} \approx (8 \text{ to } 13) \text{ TeV}. \tag{2.53}$$

It should be noted that although the range of Λ_{eq} probed is apparently smaller than that accessible in pp collisions (2.51), there it would not be possible to unravel the helicity structure of any observed contact term with the clarity possible in ep collisions.

Another important test of compositeness in ep collisions is the search for an e^*, produced by $e + \gamma$ collisions and itself decaying into $e + \gamma$. Using the effective interaction (2.48) with $g = e$ and $\Lambda^* = m_{e^*}$, it can be estimated that there is an observable rate up to

$$m_{e^*} \approx 1.5 \text{ TeV} \tag{2.54}$$

in ep collisions at $E_{cm} = 1.8$ TeV [55]. This is one case where the higher centre-of-mass energy overcomes the luminosity advantage of the lower-energy ep option.

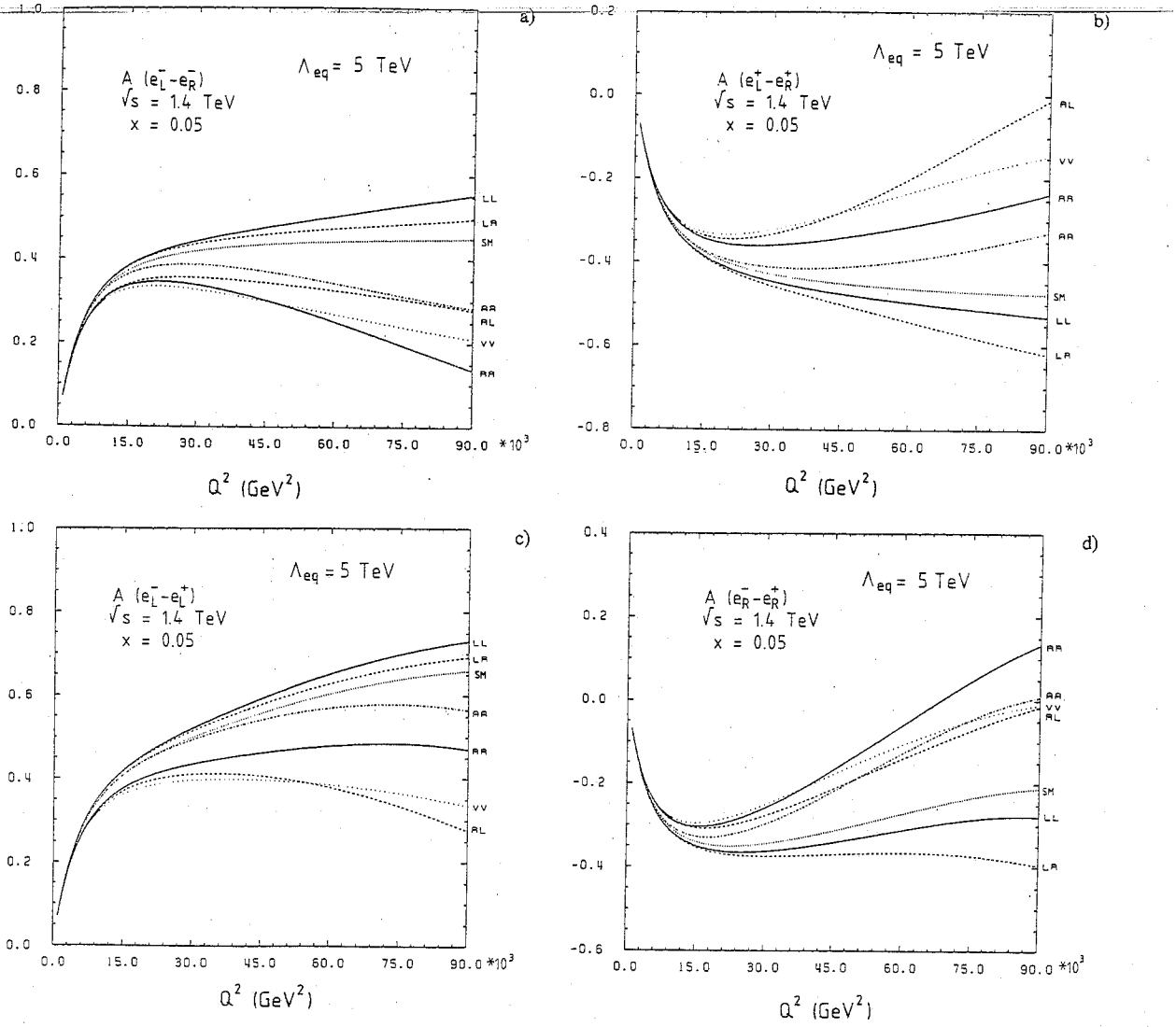

Fig. 26 Expected asymmetries [55] in ep collisions assuming Λ = 5 TeV at $\sqrt{s}$ = 1.4 TeV and x = 0.05 for a) $A(e_L^- - e_R^-)$, b) $A(e_L^+ - e_R^+)$, c) $A(e_L^- - e_L^+)$, and d) $A(e_R^- - e_R^+)$. The Standard Model predictions are also plotted.

Table 8

Expected values [55] of Λ_{eq} for the most sensitive asymmetry for each helicity combination in ep collisions

Helicities	Asymmetries	Λ_{eq} (TeV)
LL	$e_L^- - e_R^-$	8
LR	$e_L^- - e_R^-$	8
RL	$e_L^+ - e_R^+$	13
RR	$e_R^- - e_R^+$	11
VV	$e_L^+ - e_R^+$	13
AA	$e_R^- - e_R^+$	10

2.4.3 Compositeness in e^+e^- collisions

One may look for ee, $e\mu$, $e\tau$, and eq contact terms in e^+e^- collisions. We have considered in detail the ee, $e\mu$, and eq cases [56, 57]. The best limits on Λ_{ee} and $\Lambda_{e\mu}$ come from the consideration of the full angular distribution $d\sigma/d\cos\Theta$; the total cross-section alone is considerably less sensitive. In general, the range of Λ_{ee} or $\Lambda_{e\mu}$ accessible is limited by the statistics available at any given E_{cm}, resulting in:

$$\Lambda \propto E_{cm}^{1/2} (\int L\, dt)^{1/4}\,, \tag{2.55}$$

so that $L = 4 \times 10^{33}\ cm^{-2}\ s^{-1}$ gives access to values of Λ a factor of 1.4 higher than $L = 10^{33}\ cm^{-2}\ s^{-1}$. With $L \propto s$, Eq. (2.55) gives $\Lambda \propto E_{cm}$. Figures 27a and 27b show the angular distributions for $e^+e^- \to e^+e^-$, $\mu^+\mu^-$ at $\sqrt{s} =$ 2 TeV for composite models with different forms of contact terms, compared with the Standard Model predictions [57]. The errors plotted correspond to a typical measurement of the angular distribution with an integrated luminosity of 20 fb^{-1}.

The 95% CL lower bounds on Λ_{ee} and $\Lambda_{e\mu}$ as determined from $d\sigma/d\cos\Theta$ at $E_{cm} = 2$ TeV are plotted as functions of the integrated luminosity in Figs. 28a and 28b, assuming positive interference and no polarization [57]. Table 9a shows the values of Λ_{ee} and $\Lambda_{e\mu}$ accessible with unpolarized beams for the various helicity combinations.

It should be noted that there is a particular (implausible) combination of helicities, called the worst-case scenario or WCS, for which interference with the Standard Model amplitude exactly cancels, and thus the accessible range of Λ is significantly smaller than for the other forms of contact terms. However, the left-right asymmetry for $e^+e^- \to \mu^+\mu^-$ with longitudinal polarization is particularly sensitive to the WCS model, as seen in Fig. 29, and

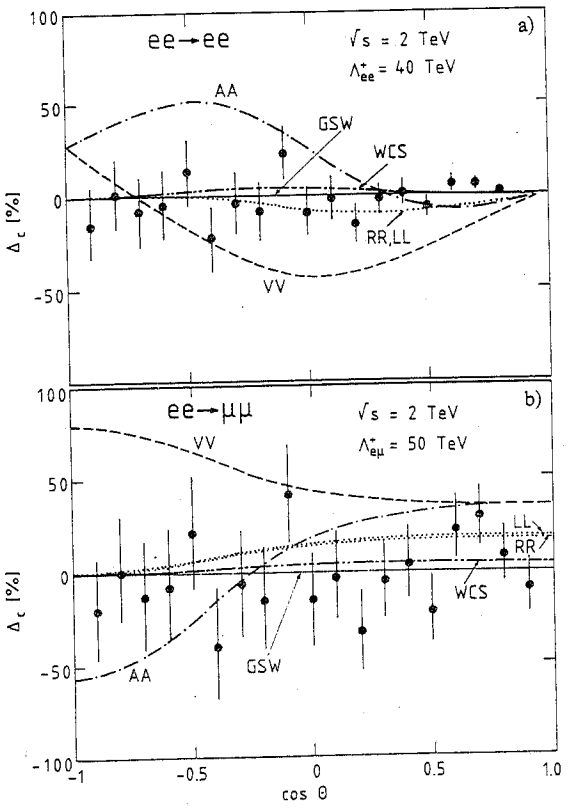

Fig. 27 Expected deviation [57] from the Standard Model predictions in the angular distribution for e^+e^- collisions at $E_{cm} = 2$ TeV and 20 fb^{-1} integrated luminosity: a) for $e^+e^- \to e^+e^-$ using $\Lambda_{ee} = 45$ TeV, and b) for $e^+e^- \to \mu^+\mu^-$ using $\Lambda_{e\mu} = 50$ TeV

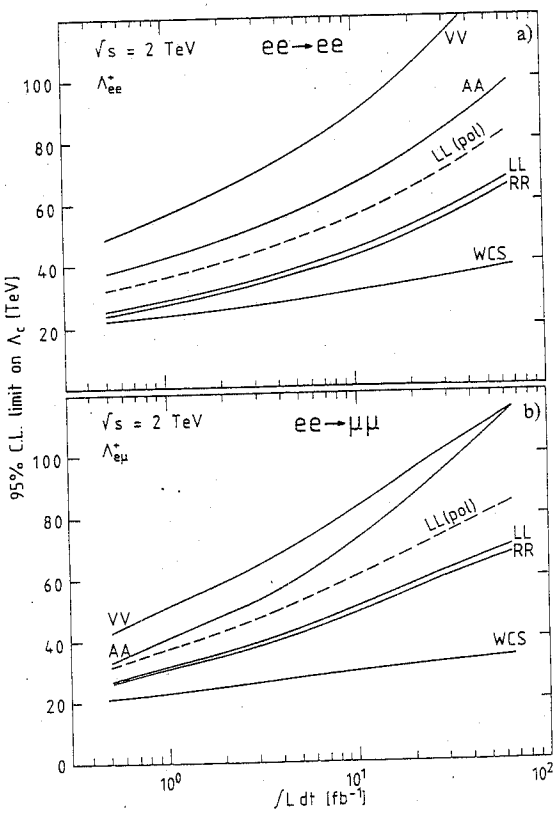

Fig. 28 Lower bounds [57] at the 95% confidence level as a function of luminosity for a) Λ_{ee} and b) $\Lambda_{e\mu}$. The curves were obtained from the $d\sigma/d\cos\Theta$ distributions without polarization, for various helicity combinations.

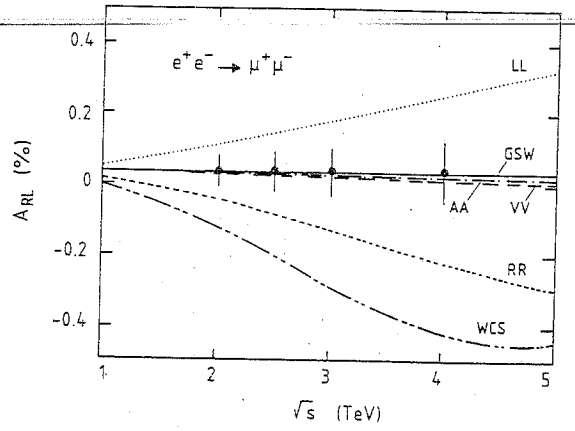

Fig. 29 Expected deviation [57] from the Standard Model predictions for a measurement of A_{RL}, assuming 50% longitudinal polarization of the e^- beam and $\Lambda_{e\mu} = 45$ TeV

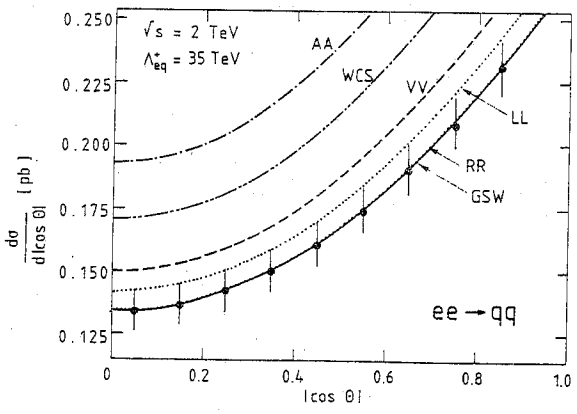

Fig. 30 Expected deviation [57] from the Standard Model prediction in the angular distribution for $e^+e^- \to q\bar{q}$ at $E_{cm} = 2$ TeV and 20 fb^{-1} integrated luminosity using $\Lambda_{eq} = 35$ TeV

Table 9

Expected 95% CL lower limits [57] on Λ_{ee} and $\Lambda_{e\mu}$ (in TeV) accessible with unpolarized and polarized beams in e^+e^- collisions at $E_{cm} = 2$ TeV with 20 fb^{-1}

	LL	RR	VV	AA	WCS
a) Unpolarized beams					
Λ^+_{ee}	49	52	104	76	34
Λ^-_{ee}	52	54	105	64	36
$\Lambda^+_{e\mu}$	56	58	95	86	32
$\Lambda^-_{e\mu}$	53	55	93	90	35
b) Longitudinally polarized beams					
Λ^+_{ee}	47	48	12	15	67
Λ^-_{ee}	47	48	12	10	67
$\Lambda^+_{e\mu}$	40	42	-	-	60
$\Lambda^-_{e\mu}$	43	44	-	-	59

gives a dramatic improvement in the accessible range of Λ, as is shown in Table 9b. On the other hand, transverse beam polarization would only give a marginal increase in the sensitivity to any of the forms of contact terms. Summarizing, the 95% confidence level limits attainable with 20 fb^{-1} at $E_{cm} = 2$ TeV are in the range

$$\Lambda_{ee}, \Lambda_{e\mu} \approx (60 \text{ to } 100) \text{ TeV}, \tag{2.56}$$

and we refer the interested reader to Table 9 and Refs. [56] and [57] for more details. These limits were obtained including a realistic systematic error of 3% in the luminosity measurement.

In the search for eq contact terms, one can hope to get information from the total cross-section and (if the quark charge cannot be measured) from $d\sigma/d|\cos\Theta|$, which provides a sensitivity identical to that obtainable from the total cross-section. In this case, the sensitivities of the bounds on Λ are mainly limited by the systematic error in the total cross-section measurement. Figure 30 shows the angular distribution for $e^+e^- \to q\bar{q}$ in e^+e^- collisions at $E_{cm} = 2$ TeV for composite models with different forms of contact terms, compared with the Standard Model predictions. As seen in Table 10, the bound on Λ_{eq} again depends on the helicity structure, and lies in the range [57]

$$\Lambda_{eq} \approx (30 \text{ to } 80) \text{ TeV}, \tag{2.57}$$

which is less than the accessible range of Λ_{ee} and $\Lambda_{e\mu}$ (2.56) but considerably exceeds the range accessible in pp or ep collisions.

Table 10

Expected 95% CL lower limits [57] on Λ_{eq} (in TeV) accessible in e^+e^- collisions at E_{cm} = 2 TeV with 20 fb^{-1}

	RR	LL	VV	AA	WCS
Λ^+_{eq}	29	33	36	55	41
Λ^-_{eq}	51	45	82	55	51

Other possible manifestations of compositeness can also be probed in e^+e^- collisions. For example, the internal structure of the W can be studied using the reaction $e^+e^- \to W^+W^-$ [58]. In the Standard Model the total cross-section for this process exhibits strong cancellation between crossed-channel ν-exchange diagrams and direct-channel (γ, Z^0) exchange diagrams. Hence it could be a particularly sensitive monitor of any deviation from the Standard Model that upsets the cancellation. (The reaction $e^+e^- \to eW\nu$ could also be a sensitive probe of such effects, but we have not studied it in detail.) The reaction $e^+e^- \to W^+W^-$ is sensitive to possible anomalies in the leptonic and bosonic sectors. In the leptonic sector, these could include form factors, an excited ν^* state, or gauge-invariant $e^+e^-W^+W^-$ contact interactions. In the bosonic sector, these could include modifications to the three-boson vertices (e.g. in the anomalous magnetic dipole moment of the W, or in the electric quadrupole moment), an excited Z^{0*} or W^* state, and non-gauge-invariant $e^+e^-W^+W^-$ contact interactions. Since the Standard Model cross-section for $e^+e^- \to W^+W^-$ is sharply peaked in the forward direction at CLIC energies, one generally finds that the most sensitive observable is the angular distribution $d\sigma/d\cos\Theta$, particularly in the backward direction. The details can be found in Ref. [58]: here we simply note that the typical sensitivity to compositeness scales entering into the specification of the new couplings is

$$\Lambda^* \approx 2E_{cm} \approx 4 \text{ TeV} \tag{2.58}$$

for CLIC with E_{cm} = 2 TeV [58]. As an example, we show in Fig. 31 the angular distributions for $e^+e^- \to W^+W^-$ in the Standard Model, including both 5% systematic and likely statistical errors, and for ν^* exchange with $\Lambda^* = m_{\nu^*}$ = 2.3 TeV at $\sqrt{s}$ = 1 TeV, assuming different helicity structures for the $eW\nu^*$ vertex.

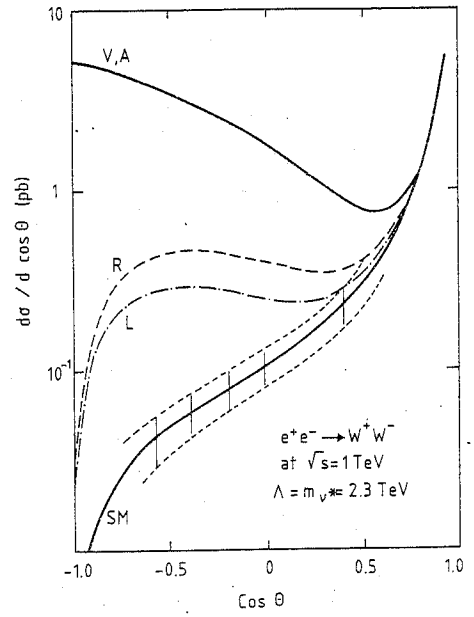

Fig. 31 Angular distributions [58] for $e^+e^- \to W^+W^-$ in the Standard Model and for ν^* exchange, assuming different helicity structures. The error bars indicate the expected systematic and statistical errors for the measurement of the angular distribution in the Standard Model.

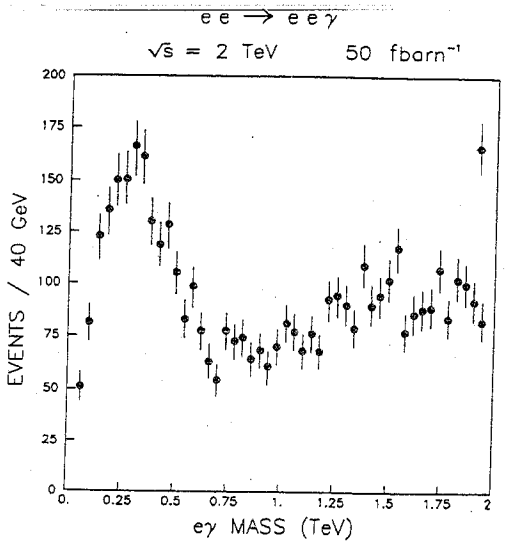

Fig. 32 The e–γ mass distribution [59] for e^* decays and QED background in e^+e^- collisions at E_{cm} = 2 TeV and 50 fb^{-1} integrated luminosity

One can also search more directly for excited states in e^+e^- annihilation. For example, using the coupling (2.48), or contact interactions, one finds that the reaction $e^+e^- \to ee^*$ produces observable numbers of e^* essentially up to the kinematic limit

$$m_{e^*} \approx 2 \text{ TeV} \tag{2.59}$$

if $\Lambda \leq 10$ TeV [59]. Figure 32 compares the signal from $ee \to e(e^* \to e\gamma)$ with the QED background for $e^+e^- \to e^+e^-\gamma$, plotted as the number of events in 40 GeV bins corresponding to the expected mass resolution [m_{e^*} = 1.92 TeV, BR($e^* \to e\gamma$) = 30%]. On the other hand, the conventional electromagnetic charge coupling of the e^* would give an observable cross-section for $e^+e^- \to e^{+*}e^{-*}$ if $m_{e^*} \leq 1$ TeV. Finally, the eeγ coupling (2.48) can also be used to probe indirectly for e^* weighing more than E_{cm} via the e^* exchange diagram contributing to $e^+e^- \to \gamma\gamma$. If $\Lambda^* = m_{e^*}$, this process is sensitive to $m_{e^*} \leq 3$ TeV.

One can also reach up to 2 TeV masses for excited quarks q^* by postulating a $qq^*\gamma$ vertex of the form (2.48) and searching for $e^+e^- \to \bar{q}q^* + q\bar{q}^*$, whilst the reaction $e^+e^- \to q^*\bar{q}^*$ gives access to $m_{q^*} \leq 1$ TeV.

In models with composite $W^\pm$ and Z^0 bosons, one generally expects i) excited Z^* bosons and ii) composite isoscalar vector bosons Y (or Y_L) coupling to the hypercharge current (or its left-handed part). At CLIC they would manifest [60, 61] themselves as resonance peaks in the e^+e^- cross-sections for $m_{Z^*,Y,Y_L} \leq 2E_{beam}$ = 2 TeV. CLIC also is sensitive [60, 61] to indirect manifestations of Z^*, Y, Y_L up to $m \approx 5$ TeV, provided their couplings to $f\bar{f}$ pairs are not much smaller than $g_{Wf\bar{f}} = 0.64$.

A consistent candidate model for composite $W^\pm$ and Z^0, the strongly coupled Standard Model, predicts correlated effects in $e^+e^- \to e^+e^-$, $\mu^+\mu^-$, $q\bar{q}$ at CLIC energies [60]. i) In the limit of exact U(12) symmetry, the reaction $e^+e^- \to e^+e^-$ would have a large peak due to the formation of a Y_L -type resonance, whilst the other reactions such as $e^+e^- \to \mu^+\mu^-$, $q\bar{q}$ would show no effect. ii) Exotic t-channel exchanges in all three reactions $e^+e^- \to e^+e^-$, $\mu^+\mu^-$, $q\bar{q}$ (due to leptoquarks, etc.) would lead to correlated dramatic deviations from the Standard Model predictions. Based on an exposure of 50 fb^{-1}, CLIC would be sensitive to masses [60]

$$m \lesssim 10\text{–}15 \text{ TeV} \tag{2.60}$$

of these exotic composites. Such bounds are well above the naturally expected mass range for partners of composite $W^\pm$ and Z^0 bosons.

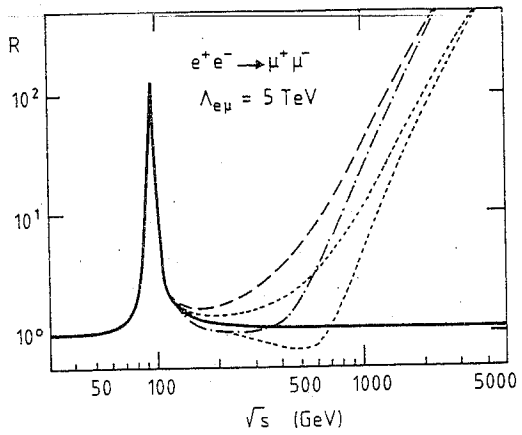

Fig. 33 Possible values [57] of R as a function of E_{cm} for $e^+e^- \rightarrow \mu^+\mu^-$ assuming $\Lambda_{e\mu} = 5$ TeV

It should be re-emphasized that most composite modellers favour a compositeness scale $\Lambda \approx 1$ to 10 TeV. If they are correct, there could be very dramatic effects in all channels at CLIC [57]. Figure 33 shows the cross-sections for $e^+e^- \rightarrow \mu^+\mu^-$ given by contact terms of the form (2.47) with $\Lambda = 5$ TeV, including a form factor to ensure damping when $E_{cm} = O(\Lambda)$. Needless to say, when E_{cm} is $O(\Lambda)$ and R becomes large, the form (2.47) of the additional interactions can be at best approximately correct. Nevertheless, there is no reason why R should not be at least as large as on the Z^0 peak. The only upper bound on R is provided by unitarity (2.29), and R could even be larger than on the Z^0 peak if there is a resonance with leptonic branching ratios larger than the 3% of the Standard Model Z^0. If the composite modellers are correct, there could be plenty of events to study at CLIC!

3. CONCLUSIONS

Each of the three accelerators we have studied has unique capabilities. We believe one should emphasize the complementarity of different machines, not a false competition between them. For example, gluinos can be studied at the LHC, but not at CLIC, whilst supersymmetric events are in general much cleaner at CLIC, and one can get more information from them. One can probe for a high-mass Z′ at the LHC, but CLIC could be used as a Z′ factory to study its properties in great detail. An ep collider produces leptoquarks singly through eq collisions, whilst the LHC and CLIC pair-produce them via conventional gauge interactions. Lepton substructure can best be probed at CLIC, whilst quark substructure can best be probed at the LHC. Moreover, there are many possibilities for physics beyond the Standard Model that we have not studied in this Working Group. Any comparison between different accelerators is necessarily subjective, since it depends on the selection of physics topics studied as well as on the quality of the measurements that can be made. This latter aspect cannot be adequately reflected in any numerical comparison.

It is with these caveats in mind that we present Fig. 34, which brings together the discovery limits for our selection of physics topics at the different accelerators. We emphasize again that the numbers presented do not tell the whole story—for example, the superior quality of supersymmetric particle searches and measurements in e^+e^- collisions is not apparent from Fig. 34.

At this meeting, the possibility has been mentioned of running the LHC at a higher luminosity, $L \geq 10^{34}$ cm^{-2} s^{-1}, for some special physics purposes. One clear example of the increased physics reach this would provide is in the search for a Z′ through its $\mu^+\mu^-$ decay. Such an increase in luminosity would enable this search to be extended to between 5 and 6 TeV. If the cross-sections for producing pairs of large-E_T jets could be measured at such a high luminosity, then the sensitivity to quark compositeness would also improve. By combining the μ and jet measurements, the discovery limit for leptoquarks $D_0 \rightarrow \mu$ + jet decays could be increased. More detailed work

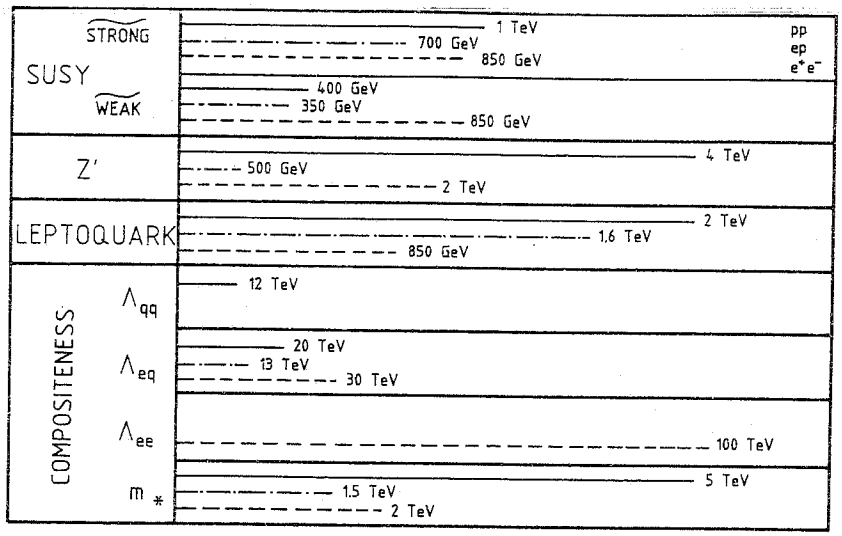

Fig. 34 Summary of discovery limits for the selected physics topics at the different accelerators discussed

would be needed to analyse whether the $\not{E}_T$ signature for supersymmetry could be seen in the multiple event environment at $L \geq 10^{34}\ cm^{-2}\ s^{-1}$.

In the case of CLIC, we re-emphasize that some important aspects of the physics would be lost if the luminosity L were to be $\leq 10^{33}\ cm^{-2}\ s^{-1}$ at $E_{cm} = 2$ TeV. The cross-sections for pair-production of scalar particles are so small that we can no longer be sure that sleptons or leptoquarks could be found. However, only a little of the sensitivity to the compositeness scale would be lost: Λ_{ee}, $\Lambda_{e\mu}$ would be reduced by $\leq 10\%$, whilst the limit on Λ_{eq} would be unchanged as this is dominated by systematic errors. Clearly any Z′ peak would be interesting at $L \approx 10^{33}\ cm^{-2}\ s^{-1}$, whilst the search for indirect effects of a Z′ with mass greater than E_{cm} would be crippled by a substantial decrease in luminosity.

It seems to us inevitable that a pp collider in the LHC/SSC range will be built in Europe and/or the United States. Such a machine certainly has very great physics capabilities, as can be seen from Fig. 34. It then becomes reasonable to ask whether a high-energy e^+e^- collider such as CLIC could offer exciting additional physics, which is not available with such a pp collider. It should be clear from the bulk of this report and from Fig. 34 that the answer is a resounding Yes! Therefore we very strongly advocate the commitment of human and financial resources to a research and development programme for CLIC along the lines suggested [11] at this meeting.

REFERENCES

[1] Proc. ECFA-CERN Workshop on a Large Hadron Collider in the LEP Tunnel, Lausanne and CERN, 1984, ed. M. Jacob (ECFA 84/85, CERN 84-10, Geneva, 1984).

[2] Proc. 1982 Summer Study on Elementary Particle Physics and Future Facilities, Snowmass, Colo., 1982, eds. R. Donaldson, R. Gustafson and F. Paige (AIP, New York, 1983).
Proc. 1984 Summer Study on the Design and Utilization of the Superconducting Super Collider, Snowmass, Colo., 1984, eds. R. Donaldson and J. Morfin (AIP, New York, 1985).
Proc. 1986 Summer Study on the Physics of the Superconducting Super Collider, Snowmass, Colo., 1986, eds. R. Donaldson and J. Marx, in preparation.
Supercollider Physics, Proc. Oregon Workshop on Super High Energy Physics, Eugene, Oregon, 1985, ed. D.E. Soper (World Scientific, Singapore, 1986).

[3] P. Langacker, Phys. Rep. **72** (1981) 185.

[4] M.E. Peskin, Proc. Int. Symp. on Lepton and Photon Interactions at High Energies, Kyoto, 1985, eds. M. Konuma and K. Takahashi (Kyoto Univ., Kyoto, 1985), p. 714.

[5] J. Ellis, New frontiers in particle physics, eds. J.W. Cameron et al. (World Scientific, Singapore, 1986), p. 225.

[6] Physics-1 Working Group, conveners G. Altarelli and D. Froidevaux, Vol. I of these Proceedings.

[7] J. Ellis, Proc. Int. Symp. on Lepton and Photon Interactions at High Energies, Kyoto, 1985, eds. M. Konuma and K. Takahashi (Kyoto Univ., Kyoto, 1985), p. 850.

[8] J.H. Schwarz, ed., 'Superstrings — the first 15 years' (World Scientific, Singapore, 1985).

[9] For reviews, see
J. Ellis, preprint CERN-TH.4439/86 (1986).
H.-P. Nilles, preprint CERN-TH.4444/86 (1986).
L.E. Ibáñez, preprint CERN-TH.4459/86 (1986).

[10] G. Brianti, Vol. I of these Proceedings.

[11] K. Johnsen, Vol. I of these Proceedings.

[12] C. Albajar et al. (UA1 Collaboration), Events with large missing transverse energy at the CERN Collider: Mass limits on supersymmetric particles (Paper III), in preparation.

[13] M. Davier, Searches for new particles, presented at the 23rd Int. Conf. on High-Energy Physics, Berkeley (1986).

[14] A. Savoy-Navarro and N. Zaganidis, Vol. II of these Proceedings.
See also S. Dawson and A. Savoy-Navarro, in Proc. Snowmass '84 (Ref. [2]).

[15] C. Dionisi, Supersymmetric particles search at LEP 200, presented at the LEP 200 ECFA Workshop, Aachen, 1986.

[16] R. Batley, Vol. II of these Proceedings.

[17] F. Paige and S. Protopopescu, ISAJET Program Version 5.23, BNL 38034 (1986).

[18] B. Mansoulié, Vol. II of these Proceedings.

[19] H. Baer, K. Hagiwara and X. Tata, Phys. Rev. Lett. **57** (1986) 294.
V.D. Angelopoulos et al., preprint CERN-TH.4578/86 (1986).

[20] H. Baer et al., Phys. Lett. **161B** (1985) 175.
H. Baer, V. Barger, D. Karatas and X. Tata, Univ. Wisconsin, Madison, preprint MAD/PH/316 (1986).

[21] Physics-3 Working Group, conveners Z. Kunszt and W. Scott, Vol. I of these Proceedings.

[22] G. Arnison et al. (UA1 Collaboration), Phys. Lett. **132B** (1983) 214.

[23] H. Komatsu and R. Rückl, Vol. II of these Proceedings.

[24] S.K. Jones and C.H. Llewellyn Smith, Nucl. Phys. **B217** (1983) 145.
P.R. Harrison, Nucl. Phys. **B249** (1985) 704.

[25] R. Cashmore et al., Phys. Rep. **122C** (1985) 275.

[26] M.E. Peskin, Physics of e^+e^- colliders: Present, future, and far future, Stanford preprint SLAC-PUB-3495 (1984).

[27] C. Dionisi and M. Dittmar, Vol. II of these Proceedings.

[28] F. Zwirner, Vol. II of these Proceedings.

[29] G. Costa et al., preprint CERN-TH.4675/87 (1987), and references therein.

[30] F. Del Aguila, M. Quirós and F. Zwirner, preprints CERN-TH.4506/86 and CERN-TH.4536/86 (1986).

[31] V.D. Angelopoulos, J. Ellis, D.V. Nanopoulos and N.D. Tracas, Phys. Lett. **176B** (1986) 203.
G. Bélanger and S. Godfrey, Phys. Rev. **D34** (1986) 1309 and TRIUMF preprint TRI-PP-86-18 (1986).
I. Bigi and M. Cvetic, Phys. Rev. **D34** (1986) 1651.
M. Cvetic and B.W. Lynn, Stanford preprint SLAC-PUB-3900 (1986).
P. Franzini and F. Gilman, Phys. Rev. **D32** (1985) 237 and Stanford preprint SLAC-PUB-3932 (1986).

[32] A. Blondel, Vol. II of these Proceedings.

[33] P. Bagnaia, Vol. II of these Proceedings.

[34] P. Chiappetta and J.-Ph. Guillet, Vol. II of these Proceedings.

[35] R. Ansari et al. (UA2 Collaboration), preprint CERN-EP/87-04 (1987), submitted to Phys. Letters.

[36] D. Froidevaux, private communication (1987); see also Ref. [6].

[37] F. Cornet and R. Rückl, Vol. II of these Proceedings.

[38] J. Ellis, Vol. II of these Proceedings.

[39] D. Schlatter, Vol. II of these Proceedings.

[40] S. Nandi, Phys. Lett. **181B** (1986) 375.

[41] D. Treille, unpublished (1987).

[42] N. Tracas and P. Zerwas, Vol. II of these Proceedings.

[43] N. Wermes, unpublished (1987).

[44] V.D. Angelopoulos et al., Ref. [19].

[45] J. Ellis and H. Kowalski, Vol. II of these Proceedings.

[46] R. Rückl and P. Zerwas, Vol. II of these Proceedings.

[47] W. Buchmüller, R. Rückl and D. Wyler, Vol. II of these Proceedings.

[48] N. Harnew, Vol. II of these Proceedings.

[49] D. Schaile and P. Zerwas, Vol. II of these Proceedings.

[50] E. Eichten, K.D. Lane and M.E. Peskin, Phys. Rev. Lett. **50** (1983) 811.

[51] A. Nandi, Vol. II of these Proceedings.

[52] G. Arnison et al. (UA1 Collaboration), Phys. Lett. **B177** (1986) 244.

[53] B. Bagnaia, N. Wermes and P. Zerwas, unpublished (1987).

[54] R. Kleiss and P. Zerwas, Vol. II of these Proceedings.

[55] F. Cornet and R. Rückl, Vol. II of these Proceedings.

[56] F. Schrempp, Max-Planck-Inst. Munich preprint MPI-PAE/PTh 69/86 (1986), to appear in Proc. 23nd Int. Conf. on High-Energy Physics, Berkeley, 1986.
B. Schrempp, F. Schrempp, N. Wermes and D. Zeppenfeld, preprint CERN-EP/87-34 (1987).

[57] N. Wermes, Vol. II of these Proceedings.

[58] P. Méry, M. Perrottet and F. Renard, Vol. II of these Proceedings.

[59] D. Bloch, Vol. II of these Proceedings and Strasbourg preprint CRN-HE 86-06 (1986).
R. Kleiss, D. Bloch and P. Zerwas, Vol. II of these Proceedings.

[60] B. Schrempp and F. Schrempp, Vol. II of these Proceedings.

[61] U. Baur, M. Lindner and K.H. Schwarzer, Max-Planck-Inst. Munich preprint MPI-PAE/PTh 74/86 (1986), and preprint in preparation.
K.H. Schwarzer, Vol. II of these Proceedings.